PERFORMANCE ASSESSMENT OF A TYPICAL RANGE HOOD VENTILATION SYSTEM

A Thesis

by

MEINAN CHEN

Submitted to the Office of Graduate and Professional Studies of
Texas A&M University
in partial fulfillment of the requirements for the degree of

MASTER OF SCIENCE

Chair of Committee,	Michael Pate
Committee Members,	Eric Petersen
	Jorge Alvarado
Head of Department,	Andreas Polycarpou

May 2015

Major Subject: Mechanical Engineering

ABSTRACT

This study assessed the real-world performance of a typical range-hood ventilation system by focusing on parameters such as duct pressure drop and range hood capture efficiency. The research can be divided into two parts, mathematical modeling and laboratory testing. For example, the pressure drop through a typical range hood ducting system and the capture efficiency of under-cabinet range hoods were modeled individually. For laboratory testing, the range hood was experimentally tested in two ducting configurations representing two typical installation strategies found in practice, namely flexible and rigid ducts exiting through walls and ceilings.

The bulk of the effort in this project was the experimental phase, and it could be divided into a Case 1 and Case 2. In Case 1 three different lengths of flexible duct (32", 46", 75") and five different lengths of rigid duct (32", 46", 75"119", 148") were mounted so as to exit a sidewall. In Case 2, rigid duct was vented through the roof by using the same duct lengths tested in Case 1. Pressure drops through the duct and vent cap were measured at different fan speed levels to produce system performance curves. These curves were overlaid with measured fan curves to find operating points (i.e. flow rate, and pressure drop) that represent real-world range-hood ventilation systems. This study provides the basis for system performance assessments and system design recommendations.

The results of this study showed that the pressure drop through flexible ducting is larger than the pressure drop through rigid ducting of same length. The increased static

pressure drop in flexible ducting had a negative impact on range hood performance, which results in a lower airflow rate and capture efficiency. By comparing the predicted and the actual results, it was found that the pressure drop measured in the experimental test is higher than that predicted by the mathematical model, which needs to be taken into consideration in future designs.

For capture efficiencies, it was found that they do not differ much for different duct lengths in the same configuration. At the same fan speed, rigid-duct range hood systems have higher capture efficiencies compared to flexible-duct range hood systems. Furthermore fan speeds have the largest effect on capture efficiencies, with values varying from 75% to 95% for fan speeds varying from low to high.

ACKNOWLEDGEMENTS

I would like to thank my committee chair, Dr. Michael Pate, and my committee members, Dr. Eric Petersen, and Dr. Jorge Alvarado, for their guidance and support throughout the course of this research.

Thanks also go to my friends and colleagues for making my time at Texas A&M University a great experience. Thanks to my dear work buddies at Riverside Energy Efficiency Laboratory, Jim, Kathryn, Solomon, Wongyu, Tony and Tiffany for all their help.

Finally, thanks to my mother and father for their encouragement .

NOMENCLATURE

ASHRAE	American Society of Heating, Refrigerating and Air-conditioning Engineers
C	Compression Ratio [%]
C_0	Constant Coefficient, 1.68E-05 [$100\ ft \cdot (cfm)^n$]
C'	Local Fitting Loss Coefficient
CE	Capture Efficiency
CFD	Computational Fluid Dynamics
CFM	Volumetric flow rate in rigid ducts [cfm]
D	Diameter [in]
DAQ	Data Acquisition
FD	Flexible Duct
HVI	Home Ventilating Institute
HVAC	Heating, Ventilation and Air-conditioning
K	Local Pressure Loss Coefficient
K'	Newly Defined Local Pressure Loss Coefficient
L	Length [in]
LBNL	Lawrence Berkeley National Laboratory
n	Constant
P	Pressure [inch WC]
ΔP	Pressure Loss [inch WC]

REEL	Riverside Energy Efficiency Laboratory
RD	Rigid Duct
$\dot{V}$	Volumetric Airflow Rate [cfm]
ρ	Standard Density of Air [$0.075 lbm/ft^3$]

TABLE OF CONTENTS

Page

ABSTRACT ii

ACKNOWLEDGEMENTS iv

NOMENCLATURE v

TABLE OF CONTENTS vii

LIST OF FIGURES ix

LIST OF TABLES xii

CHAPTER I INTRODUCTION 1

Overview 1
Purpose and Goals of Study 3
Scope of Work 4
Mathematical Modeling Overview 4
Experimental Tests and Analysis Overview 4

CHAPTER II BACKGROUND THEORY 8

System and Fan Curves and Operating Points 8
Range Hood Performance Ratings 10
Flexible Duct Compression Ratio 11
Capture Efficiency 11

CHAPTER III LITERATURE REVIEW 13

Previous Research on Flexible Ducts 13
Previous Research on Capture Efficiency 15
Previous Research on Vent Caps 16

CHAPTER IV MATHEMATICAL MODELLING 17

Pressure Drop in Flexible Duct 17
Pressure Drop in Rigid Ducts and Bends 20
Pressure Drop through Wall Vent Caps 22
Total System Pressure Drop Model 23

Capture Efficiency of Residential Cooking Exhaust Hoods 24

CHAPTER V TEST METHODOLOGY 28

Field Trip: Present Day Range Hood Ducting System 28
Airflow Test 30
Airflow Test Setup 30
Airflow Test Procedure 34
Range Hood Ducting System Pressure Drop Test Setup 36
Tests Description and Preparation 36
Static Pressure Measurement 37
Case 1 Setup 41
Case 2 Setup 44
Data Acquisition and Instrumentation 46
Test Procedure 51

CHAPTER VI RESULTS AND DATA ANALYSIS 53

Airflow Tests and Fan Curves 53
System Curves and Operating Points 55
Test Results for Case 1 and Case 2 55
Predicted Pressure Loss for Case 1 and Case 2 57
Comparison between System Curves for Case 1 and Case 2 60
Comparison between Operating Points for Case1 and Case 2 62
Impact Analysis 68
Capture Efficiency 71

CHAPTER VII CONCLUSIONS 75

REFERENCES 78

APPENDIX A 80

APPENDIX B 81

APPENDIX C 82

APPENDIX D 84

APPENDIX E 85

LIST OF FIGURES

Page

Figure 1. Two Approaches for Venting a Range Hood....3

Figure 2. Actual System Curve, Designed System and Fan Curve (ASHRAE, 2005a) 9

Figure 3. Pressure Drop Correction Factors for Flexible Duct (ASHRAE, 2005a).....14

Figure 4. Averaged Loss Coefficient versus Compression Ratio for Flexible Ducts 19

Figure 5. Three Gore, 90 Degree Elbow, Diameter=6" (ASHRAE, 2005a).....21

Figure 6. Loss Coefficient versus Airflow Rate for 6" Vent Caps (Escatel, 2011) 23

Figure 7. Capture Efficiency at Different Airflow Rates (Delp, 2012).....26

Figure 8. (a) Rigid Duct Vented Through Sidewall; (b) Rigid Duct Vented Through Roof; (c) Flexible Duct Vented Through Sidewall in Some Apartments 29

Figure 9. Green Airflow Test Chamber Located at REEL.....31

Figure 10. Nozzle Board Layout for the Green Air Flow Chamber 32

Figure 11. HVI Standard 916 Standard Test Setup for an Outlet Chamber.....33

Figure 12. Range Hood Airflow Test Setup.....33

Figure 13. Airflow Test Program Operation Interface.....34

Figure 14. Zero Pressure Transducers Panel.....35

Figure 15. Case 1 (Flexible Duct) Pressure Measurement Test Setup.....37

Figure 16. Pressure Tap Illustration.....38

Figure 17. A Well Made Pressure Tap Following Standards.....38

Figure 18. A Pressure Ring on a Round Duct.....39

Figure 19. Dimension of the Separate Fixed Pressure Ring.....40

Figure 20. Pressure Ring on the Vent Cap.....41

Figure 21. Case 1 Test Setup Dimension (Flexible Duct)....43

Figure 22. Flexible Duct Fastened to Shelving with a Rubber Attachment....43

Figure 23. Case 1 (Wall Vent) Test Setup Dimension (Rigid Duct)....44

Figure 24. Case 2 (Roof Vent) Test Setup Dimension (Rigid Duct) 46

Figure 25. DAQ System....47

Figure 26. Pressure Sensor Board 48

Figure 27. Sensors Wiring Diagram....49

Figure 28. LabVIEW Program Front Panel 50

Figure 29. Block Diagram in LabVIEW Program 51

Figure 30. Measured Fan Performance Curves at Different Fan Speeds 54

Figure 31. Measured RPM versus Airflow Rate at Different Fan Speeds 54

Figure 32. Comparison between System Curves for Case 1 (Flexible Ducts)....61

Figure 33. Comparison between System Curves for Case 1 (Rigid Ducts) 61

Figure 34. Comparison between System Curves for Case 2 (Rigid Ducts) 62

Figure 35. Comparison between Operating Points for Case 1 (Flexible Ducts) 63

Figure 36. Comparison between Operating Points for Case 1 (Rigid Ducts) 64

Figure 37. Comparison between Operating Points for Case 2 (Rigid Ducts) 64

Figure 38. Comparison between Operating Points for 75" Duct Length in Case 1 (Rigid Duct) 65

Figure 39. Comparison between Operating Points for 75" Duct Length in Case 2 (Rigid Duct)....65

Figure 40. Comparison of Operating Points for Case 1 and Case 2....67

Figure 41. Actual and Predicted Pressure Loss for Components and Total System for 75" Duct Length in Case 1 (Flexible Duct) 69

Figure 42. Actual and Predicted Pressure Loss for Components and Total System for 75" Duct Length in Case 1 (Rigid Duct).....70

Figure 43. Comparison of Individual Component Impact 71

Figure 44. Capture Efficiency for Flexible Ducts (Case 1).....73

Figure 45. Capture Efficiency for Rigid Ducts (Case 2).....73

Figure 46. Comparison of Capture Efficiency between Flexible and Rigid Ducts.....74

Figure 47. Data Used for Developing Pressure Drop Mathematical Model 80

Figure 48. Manometer Used for Reference Pressure Supply 82

Figure 49. Tube Connection for Pressure Calibration.....83

Figure 50. Test Setup for Case 2 84

Figure 51. Actual and Predicted Pressure Loss for Components, and Total System for Case 1, (a) 32" Flex Duct; (b) 46" Flex Duct; (c) 32" Rigid Duct, (d) 46" Rigid Duct, (e) 119" Rigid Duct, (f) 148" Rigid Duct.....87

LIST OF TABLES

Page

Table 1. Measured Experimental Data for the Range Hood Ventilation System 5

Table 2. Performance Assessment of US Residential Cooking Exhaust Hoods.....26

Table 3. Green Air Flow Chamber Nozzle Information 32

Table 4. Detailed Information of the Sensors 48

Table 5. Test Results for Case 1 (Sidewall Vent Cap).....56

Table 6. Test Results for Case 2 (Through Roof Vent Cap) 56

Table 7. Predicted Pressure Loss for Case 1 (Flexible Ducts) 58

Table 8. Predicted Pressure Loss for Case 1 (Rigid Ducts) 58

Table 9. Predicted Pressure Loss for Case 2 (Rigid Ducts) 59

Table 10. x and y Value of Operating Points for Each Case.....67

Table 11. Capture Efficiency for Case 1 72

Table 12. Capture Efficiency for Case 2 72

CHAPTER I

INTRODUCTION

Overview

Heating, ventilation and air-conditioning (HVAC) system design is the most complex topic in house designing (Burdick, 2011), when one considers that the energy consumption of the whole house, involves predicting house heating and cooling loads, selecting equipment of the right size, duct design to match equipment and finding blower fan capabilities. In addition to energy consumption considerations, an effective HVAC system design must also guarantee that properly conditioned air is delivered to a space efficiently for health and safety reasons. In this regard, the kitchen ventilation system is an important branch of a whole-resident ventilation system, which is the subject of this thesis.

According to many building regulations, a kitchen must be provided with a window opening that connects to outdoor air. This alone is not an effective way to remove the moisture, smell, contaminants, and carbon dioxide that is generated during the cooking process. On the contrary, it can even help spread contaminants into other parts of a residential building because of wind effects. Therefore many households equip their kitchens with a range exhaust hood, which is a device containing a mechanical fan that hangs above the stove in the kitchen. Its main function is to remove pollution, such as combustion products, smoke and steam from the air by evacuation of the air through a

filtration system, and then keeping the pollution level in a confined space as low as possible.

Range hoods can be divided into two main categories. The first category is a recirculating range hood or ductless range hood, which recirculates air from the stove top back to the kitchen, so that filters may be needed to remove odors and grease. The other category, which is the focus of this study, is when the range hood exhausts air to the outdoors and ensures that fresh air comes back into the room.

There are two approaches to installing range hood ductwork as shown in Figure 1, with one being through the sidewall while the other is through the roof. When installing a range hood, the length of the ductwork is a main consideration, usually a longer ductwork with more bends will require a higher fan discharge pressure, which is provided by the range hood, in order to overcome the ductwork resistance. Both flexible ducts and rigid ducts are used in a ductwork for range hood, and vent caps are used at the interface between the ducting and the outdoor, to make sure the air flows into the ambient while not allowing the same air to return into the building.

There are various kinds of flexible ducts available in residential applications, such as metallic flexible ducts and nonmetallic flexible ducts. Flexible ducts are widely used in practice due to its flexible nature, allowing for easy installation and an ability to be installed in confined spaces. However, rigid ducts are more sturdy and less likely to have leaks, which would be a safety issue.

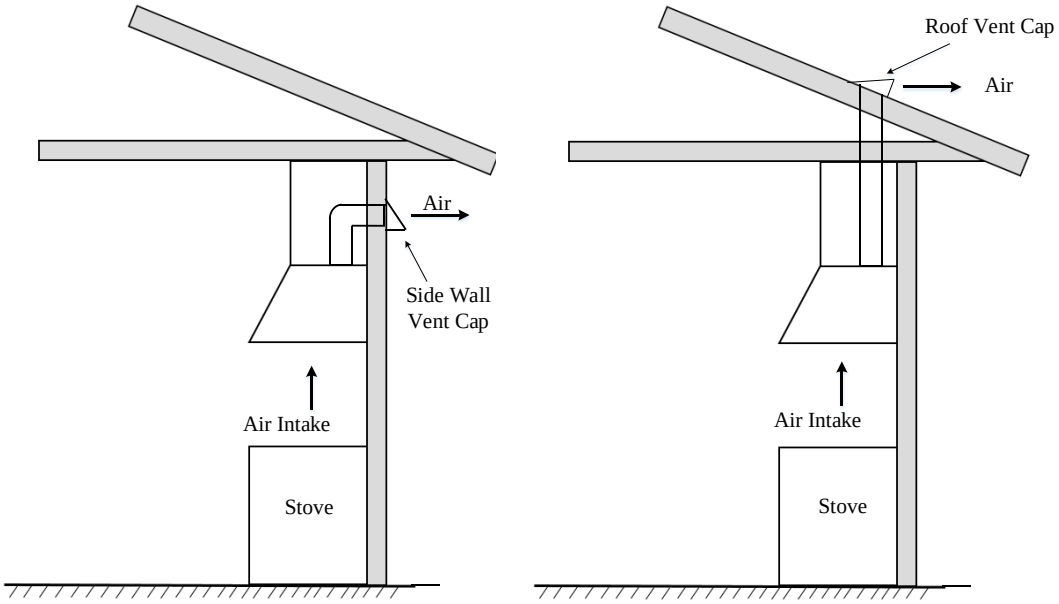

Figure 1. Two Approaches for Venting a Range Hood

Purpose and Goals of Study

Range-hood fan airflow rates have been measured previously in laboratory studies; however, the results are not applicable to real-world applications, because these past studies have not indicated the ducting and vent caps. Therefore the purpose of this study is to evaluate the performance of range-hood fans in real-world systems that include ducts and vent caps. In this respect, the laboratory fan data (i.e. fan curves) and real-world ducting and vent cap data (i.e. system curves) measured in this study is combined to perform an analysis and assessment, which can then be used by HVAC designers. Furthermore, because the purpose of the range hood is to remove contaminants, the real-world range-hood capture efficiency can then be determined by combining the experimental data reported in this thesis with the capture efficiency

versus flow rate data measured previously by Lawrence Berkeley National Laboratory (LBNL).

Scope of Work

The research work in this study can be divided into two parts, namely mathematical modeling and experimental tests.

Mathematical Modeling Overview

Firstly, pressure drops through individual components, including flexible ducts, rigid ducts, bends, and vent caps will be modeled individually. For the flexible and rigid duct component, the modeling will utilize data from previous Texas A&M University research performed on pressure drops through flexible ducts (Weaver, 2011). For the bends, pressure drops will be modeled by utilizing ASHRAE published data in ASHRAE Handbook 2005 (ASHRAE, 2005A). For the pressure drop models through the vent caps, research results from a former REEL student Escatel will be used (Escatel, 2011). Secondly, mathematical modeling of range hood capture efficiency for back burner configurations will use data based on LBNL research results (Delp, 2012).

Experimental Tests and Analysis Overview

In the experimental part of the project, airflow tests will first be performed on range hood fans by using the Riverside Energy Efficiency Laboratory flow chamber, which can be used to obtain air flow rate data versus pressure drop data to create fan performance curves. After obtaining fan curve data in the lab, experiments will be performed on well-unstructured real-world range hood and duct assembly systems that duplicate actual systems installed in residential households. Furthermore, these

experiments will be performed on the two configuration approaches for installing range hood systems, either exhausting through the sidewall or through the roof. In Configuration 1 through the sidewall, flexible ducting is connected to the range hood outlet and tested at three different lengths (32”, 46”, 75”), and then changed to rigid ducting to be tested at 5 different lengths (32”, 46”, 75”119”, 148”). In Configuration 2 through the roof, only rigid ducting is tested at 5 different lengths, which are the same as those in configuration 1. For each test, pressure drops through the duct and vent cap system are measured and a system curve is generated for each duct length to then be superimposed on previously measured fan curves. The test matrix and data to be taken is shown in Table 1, with P1 being the pressure drop through the ducting system, while also includes a bend, and P2 being the pressure drop through the vent cap mounted at the outlet.

Table 1. Measured Experimental Data for the Range Hood Ventilation System

	Duct Type	Duct Length (inch)	Speed	P1(inch WC)	P2(inch WC)	Rotational Speed (rpm)	Airflow rate (cfm)
Case 1 (Through sidewall)	Rigid Duct	32	High	x	x	x	x
			Medium	x	x	x	x
			Low	x	x	x	x
		46	High	x	x	x	x
			Medium	x	x	x	x
			Low	x	x	x	x
		75	High	x	x	x	x
			Medium	x	x	x	x
			Low	x	x	x	x

Table 1. Continued

	Duct Type	Duct Length (inch)	Speed	P1(inch WC)	P2(inch WC)	Rotational Speed (rpm)	Airflow rate (cfm)
Case 1 (Through sidewall)	Rigid Duct	119	High	x	x	x	x
			Medium	x	x	x	x
			Low	x	x	x	x
		148	High	x	x	x	x
			Medium	x	x	x	x
			Low	x	x	x	x
	Flexible Duct	32	High	x	x	x	x
			Medium	x	x	x	x
			Low	x	x	x	x
		46	High	x	x	x	x
			Medium	x	x	x	x
			Low	x	x	x	x
		75	High	x	x	x	x
			Medium	x	x	x	x
			Low	x	x	x	x
Case 2 (Through roof)	Rigid Duct	32	High	x	x	x	x
			Medium	x	x	x	x
			Low	x	x	x	x
		46	High	x	x	x	x
			Medium	x	x	x	x
			Low	x	x	x	x
		75	High	x	x	x	x
			Medium	x	x	x	x
			Low	x	x	x	x
		119	High	x	x	x	x
			Medium	x	x	x	x
			Low	x	x	x	x
		148	High	x	x	x	x
			Medium	x	x	x	x
			Low	x	x	x	x

Of special importance and as noted previously, the fan curves and system curves can be overlapped (i.e. superimposed) to find the real-world operating point (flow rate

and pressure drop point). In addition, the measured system curve can be compared to the system curve generated from mathematical modeling, and as a result, design considerations well beyond what can be measured in the laboratory can be investigated.

CHAPTER II

BACKGROUND THEORY

System and Fan Curves and Operating Points

A fan performance curve depicts the relationship between the static pressure and airflow rate at a given operating speed with each operating speed having a corresponding fan curve. Of special importance, the pressure-flow rate performance of a fan can be predicted based on fan curves, and, as such, fan manufacturers provide their customers with airflow fan test data in a table on graph with their products. Their airflow test data (i.e. fan curve data) for fans is usually measured in a laboratory system following the Home Ventilating Institute (HVI) airflow test standard 916 (HVI, 2009), which specifies standard testing and rating procedures in accordance with ANSI consensus standards.

A system resistance curve represents how a system pressure drop reacts to a given airflow. For example, the flow resistance for a range hood ventilation system includes pressure losses through the ducting (rigid ducts or flexible ducts), elbows, bends, wall or ceiling vent caps and any other fitting that involves a resistance to airflow.

The intersection point of the fan performance curve and the system curve is called the operating point, and the actual airflow rate and pressure drop is determined by the operating point. Therefore, the air flow of the installed kitchen-hood exhaust device depends on the performance curve of the fan and the flow resistance through the venting system. Fan curves are necessary for fan selection, and when the operating speed is

given, fan performance characteristic always follow the fan curve. There are two main considerations for selecting a fan for any system. One important consideration is to select a fan that gives the airflow rate needed for overcoming a system pressure drop, which means that the pressure drop through the system must be known for fan selection. Another consideration is to select a fan that has its peak efficiency at or near the operating point. Figure 2 taken from ASHRAE Handbook (ASHRAE, 2005a) shows the relationship between an actual system curve, a predicted system curve and a fan curve, as well as the actual and designed operating points.

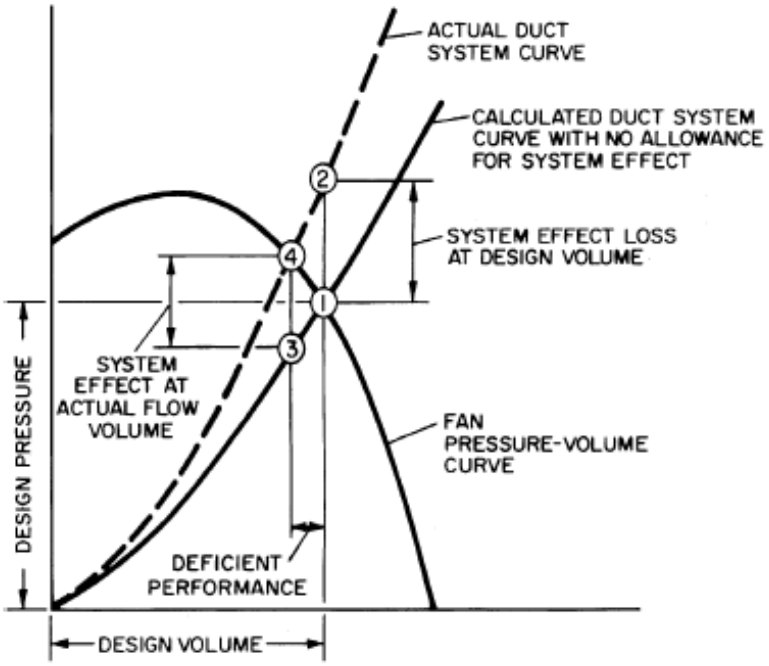

Figure 2. Actual System Curve, Designed System and Fan Curve (ASHRAE, 2005a)

Range Hood Performance Ratings

There are multiple criteria to evaluate the performance of a range hood: airflow, loudness, power consumption, and capture efficiency. Home Ventilating Institute (HVI) has established a standard rating system for airflow testing, sound testing and power consumption measurement; however, there is no standard rating system for the capture efficiency, which is defined as the percentage of emissions captured and vented to a control device.

Every year HVI publishes airflow and sound test results for a wide variety of fans and range hoods in HVI certified Products Directory, which is necessary for comparing fans and for aiding with range hood selections. Usually the airflow rating point is 0.1 inch WC and 0.25 inch WC for fans, and 0.1 inch WC for range hoods, where WC stands for water column.

The HVI test standard specifies that range hood fans will be tested and rated at a static discharge pressure of 0.1 inch WC, meaning that the rated airflow in cfm for the fan is based on this pressure across the fan. The explanation of this test point is that the system containing the fan will have a flow resistance or pressure drop similar to 0.1 inch WC for the given flow rate. However, in practice, the rating point of 0.1 inch WC cannot always represent the real-world situation. For example there are numerous other factors that need to be taken into consideration, such as elbows, flexible ducts, transitions, and vent caps, with all attributing to the flow resistance. To summarize, the rating point is a guide for comparing hoods; however, in real applications, the actual installation will influence the performance of the hood, which will always be different

from the rated performance. Furthermore, even though the purpose of the range hood is to remove contaminants, there is no standard testing method for measuring or determining the capture efficiency of range hoods. As a result there is no connection between capture efficiency and the rated condition and even more importantly, real applications under real-world conditions need to be considered to obtain the actual capture efficiencies, which is the subject of this thesis.

Flexible Duct Compression Ratio

Pressure drops through flexible ducts are more complex than pressure drops through rigid ducts because flexible ducts have compressibility characteristics, based on a compression ratio which describes how compressed a flexible duct is. The compression ratio can be defined as the change in length after being compressed divided by the fully stretched length. It is known that pressure losses in flexible ducts increase as the duct is compressed, but there is no uniform or established relationship between pressure loss and other parameters such as duct diameter, compression ratio and airflow rate.

Capture Efficiency

Cooking pollutants emitted from burners can reach a hazardous level for indoor air and can do harm to human health. It is necessary to remove the cooking contaminants to maintain indoor air quality and to ensure a healthy life. A measure of a range hood's ability to remove contaminants is the capture efficiency, which defined as the percentage of total emissions that are captured and vented to a control device (i.e. range hood and fan). Specifically, for a range hood venting system, capture efficiency is the fraction of pollutants removed by the exhaust fan divided by the total amount of pollutants

generated from the cooking device. Range hood capture efficiency varies with range hood type, fan speed, burner configurations, and even contaminant types. There are no standard rating systems for range hood capture efficiency performance, which is surprising given that the purpose of the range hood is to remove contaminant.

CHAPTER III

LITERATURE REVIEW

Certain areas addressed in the study presented here have been well-covered and established over the years and are well known in the HVAC engineering field. However, other areas to be modeled and experimentally tested in this research are unique and less well known. Therefore, three of these less known but important areas pertinent to this study are presented in this literature review chapter, including pressure drops through flexible ducts and vent caps, as well as range hood capture efficiencies.

Previous Research on Flexible Ducts

In 2004, researchers at LBNL performed a study to evaluate the influence of compression ratios on pressure drops in flexible, spiral wire helix core ducts (Abushakra, 2004). Tests were conducted on 6", 8" and 10" ducts with different compression ratios and it was found that the published data in the literature underestimate the compression effects. They then developed pressure drop power-law and the pressure drop correction factor models (PDCF) to predict pressure drop for different compression ratio. In 2005 ASHRAE Handbook Fundamentals Chapter 35, Duct Design (ASHRAE, 2005a) presented a chart, which is Figure 3, that shows pressure drop correction factors for straight, flexible ducts that are less than fully extended. This ASHRAE chart used the research results obtained previously by Abushakra (Abushakra, 2004).

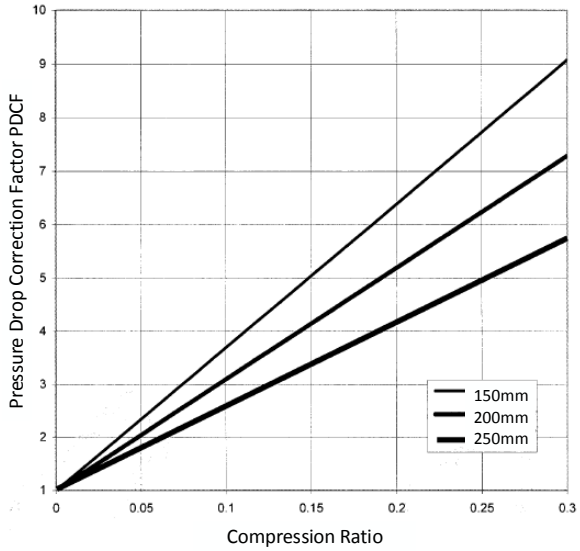

Figure 3. Pressure Drop Correction Factors for Flexible Duct (ASHRAE, 2005a)

Another study measured airflow static pressure losses through non-metallic flexible ducts with diameters of 6", 8" and 10" and a range of compression ratios 4%, 15%, 30%, 45% and 100% of maximum stretch, (Weaver, 2011). The testing configurations were expanded by using an as-built test protocol, including maximum stretch, board supported, joist supported, joist natural sag and joist long term sag. The results showed that when the compression ratio is above 4%, the configuration has a great influence on duct performance. Later, a CFD simulation study was performed on the 30% compressed case (Uğursal, 2006), the simulation results present close comparison with testing results.

A final study reported static pressure losses in 12", 14" and 16" non-metallic flexible ducts that were tested at five different compression ratios, namely 4%, 15%, 30%, 45% and 100% of maximum stretch (Cantrill Jr, 2013). The results showed good

agreement with previous studies in that the flexible duct performance decreased with an increase in compression ratio. This latest flexible duct study is less appropriate to the study reported here, because the duct diameters are all much larger than those typically found in range hoods.

Previous Research on Capture Efficiency

Lawerence Berkeley National Laboratory (LBNL) has reported and conducted extensive research on studying range hood capture efficiencies starting in 2011, with a web-based survey gathering information about cooking appliance use in California homes (Klug, 2012). These results were used to set up an experimental study of capture efficiency (Singer, 22.3 (2012)). LBNL then performed experimental tests on fifteen cooking exhaust devices as installed in residences with regards to their ability to remove contaminants. Their experimental results were then analyzed and compared in order to quantify the impact of different parameters (range hood type, air flow rate, burner configuration) on capture efficiency. In addition to converting and analyzing their data results in a series of plots, they also found that the back burner configurations with open range hoods have the highest capture efficiency performance.

In another LBNL study, laboratory tests were conducted on seven new under-cabinet hoods representing typical U.S design in order to assess range hood performance with regard to removing contaminants (Delp, 2012). Capture efficiency was measured for three burner configurations: both back burners, both front burners, and the oven. It was found that open hoods using back burner configurations have the highest capture efficiency, which is consistent with previous test results.

Previous Research on Vent Caps

In 2011, extensive tests were performed on a wide variety of vent caps to evaluate vent caps performance over a wide flow rate range (Escatel, 2011). The pressure drop versus airflow rate relationship was measured for vent caps of different types, designs, and sizes. Soffit, wall-mount and roof jack vent caps of 4” and 6” were tested. The pressure drops across the vent caps for a range of flow rates were used to calculate nondimensional loss coefficients, with the results showing that loss coefficients can be used to predict pressure drops across vent caps over a range of air flow rates.

CHAPTER IV

MATHEMATICAL MODELLING

The first modeling step is to determine those components and their characteristics to be modeled and then to identify those mathematical equations that govern the component's behavior. There are several major components in a range-hood ducting system that can affect the system performance., including flexible or rigid ducts, vent caps, and bends Each of these components are modeled here individually, and then combined to form a system model utilizes a capture efficiency model to fully evaluate the efficiency of range hood system along with the ducts to remove contaminants when operating real-world conditions.

Pressure Drop in Flexible Duct

A study by Weaver (Weaver, 2011) suggests that the pressure drop through metallic flexible ducts is comparable with that through non-metallic flexible ducts. Because there are no available references for pressure drops through metallic flexible duct, as was used in this study, the testing results of non-metallic flexible ducts reported by Weaver (Weaver, 2011) were then used to generate pressure drop model with compression effects. As noted, the modeling equation used to calculate pressure loss at a given air flow rate for a given duct size was developed based on the testing results reported by Weaver (Weaver, 2011), where the loss coefficient is defined as

$$\Delta P = K \cdot \frac{L}{D} \cdot \frac{\rho V^2}{2} \tag{1}$$

and,

$$K = \frac{\Delta P}{\frac{1}{2}\rho V^2 \frac{L}{D}} \tag{2}$$

In the above equations, the parameter L is the length of pipe, D is the hydraulic diameter for the pipe, V is the average velocity of the fluid flow, and ΔP is the pressure loss. Furthermore the loss coefficients for 6 inch diameter flexible ducts used in this thesis can be defined by using duct diameter and airflow rate as follows.

$$K' = \frac{\Delta P D^4}{\rho \dot{V}^2} \tag{3}$$

ΔP Pressure loss (inch WC/100ft)

D Duct diameter (inch)

ρ Standard density of air ($0.075 lbm/ft^3$)

$\dot{V}$ Air flow rate (cubic feet per minute, cfm)

In the flexible duct model used here, the value of K' was calculated by using Eq. 3 based on test data taken from Weaver (Weaver, 2011). In that study, several configurations were tested, but it is assumed that the flexible duct installations are straight, with board supports, which all the test result used for the calculation of K' here. The K' values from Weaver (Weaver, 2011) for different duct sizes at various air flow rate are listed in Appendix A. It was found that K' values are comparatively stable at different air flow rates; however, the values are sensitive to duct diameter and compression ratio. Therefore, for use here, a general model for flexible ducting was developed by averaging K' values at different airflow rates over all these duct sizes. By

adding and averaging linear trend lines for the three duct sizes, it was found that there is approximately a linear relationship between K' and the compression ratio for any given duct size. By comparing the pressure drop predicted by the flexible duct model averaged over all diameters with testing data, the general model was shown to have a large error of more than 20%, meaning that it is not appropriate for ducting system pressure drop modeling. Therefore as a next step, an individual model was developed for each duct size (6", 8" and 10") based on the linear relationship between K' and compression ratios. For example, as shown in Figure 4, the 6 inch duct, which is the duct used in the thesis study, the loss coefficient equation is $K' = 0.0551 * C + 0.1635$. The resulting pressure drop mathematical model, which also includes the above loss coefficient equation, for 6" flexible duct is shown in Eq.4, this is the mathematical model that can be used to calculate pressure drop as a function of flow in the flexible ducts found in this study.

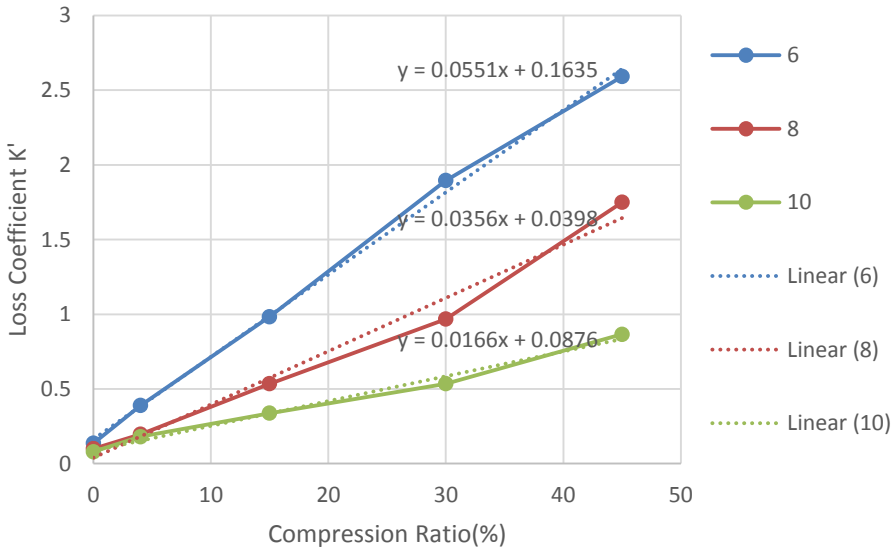

Figure 4. Averaged Loss Coefficient versus Compression Ratio for Flexible Ducts

$$\Delta P = \frac{(0.0551C + 0.1635)\rho \dot{V}^2}{D^4} \quad (4)$$

ΔP Pressure loss per 100 feet length of flexible duct (inch WC/100ft)

C Compression ratio (%)

D 6" Duct diameter (inch)

ρ Standard density of air ($0.075 lbm/ft^3$)

$\dot{V}$ Air flow rate (cubic feet per minute, cfm)

Pressure Drop in Rigid Ducts and Bends

Pressure losses in rigid sheet metal ducts were modeled by using a power law equation, Eq. 5 as follows (Weaver, 2011).

$$\Delta P = C_0 \cdot (cfm)^n \quad (5)$$

where

ΔP Pressure drop through rigid duct (inch WC/100feet)

C_0 Constant coefficient, 1.68E-05 ($100\ ft \cdot (cfm)^n$)

cfm Volumetric flow rate in rigid ducts, cfm

n Constant equals, 1.84

For bends in rigid ducts, pressure losses were modeled by using the relationship given in Eq. 6.

$$\Delta P = C' \cdot \frac{\rho V^2}{2} \quad (6)$$

where ΔP is pressure loss due to friction (Pa); C' is the bend loss coefficient; ρ is fluid density (kg/m^3), and V is the mean flow velocity (m/s). After converting to British units, inputting parameter values, and introducing new parameters, then the original Eq.4 become the following equation, Eq. 7.

$$\Delta P = C' \cdot \frac{\dot{V}^2}{617234} \tag{7}$$

Where

ΔP Pressure loss in a duct (inch WC)

$\dot{V}$ Volumetric flow rate in the bends (cubic feet per minute, cfm)

C' Local fitting loss coefficient

Fitting loss coefficients for sheet metal bends are listed in the Duct Fitting Database in ASHRAE Handbook, fundamentals, Chapter 35 (ASHRAE, 2005a). The rigid duct bend used in the tests reported here, is a 90 degree elbow with three gores, and the r/D equal to 1.5 as shown in Figure 5. According to the database, the approximate loss coefficient for this type of bend is equal to 0.34.

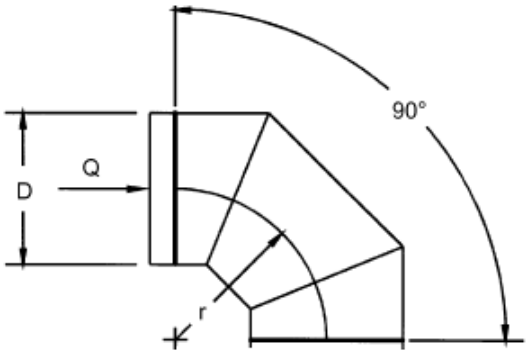

Figure 5. Three Gore, 90 Degree Elbow, Diameter=6" (ASHRAE, 2005a)

Abushakra (Abushakra, 2002) showed that for bends in flexible ducts, there was big variance in loss coefficient with different conditions, which could not be calculated or summarized uniformly. In 2005 the ASHRAE Handbook, it is suggested to use 2.0 for any bend in flexible ducts.

Pressure Drop through Wall Vent Caps

Pressure drops across the vent caps installed at the system exit were modeled by using the data and analysis reported by Escatel (Escatel, 2011), who tested both 4" and 6" vent caps, with the later diameter being the same as that used in this thesis study. Figure 6 shows loss coefficient changing with flow rate for 6 inch vent caps with labels Q to V representing a variety of wall-mounted vent cap types, and W and X representing two types of roof-mounted vent caps. It can be seen that when most airflow rates are above 100 cfm, then the loss coefficients for 6-inch vent caps are mostly constant, which can be used to calculate pressure drop through vent caps when airflow rate is above 100 cfm.

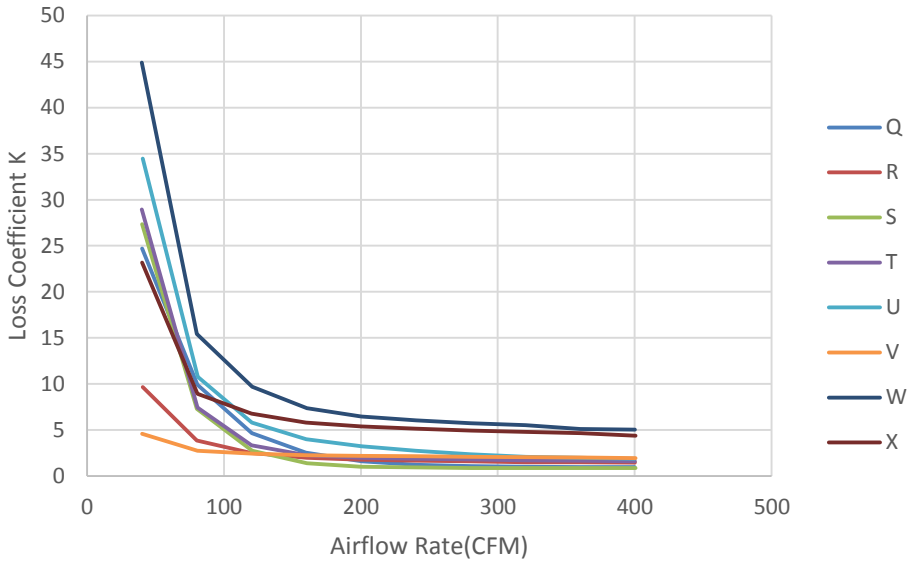

Figure 6. Loss Coefficient versus Airflow Rate for 6" Vent Caps (Escatel, 2011)

Using the results in Figure 6 at flow rates above 100 cfm, an average K value of 1.48 for the six wall-mounted vent caps was used for the vent cap pressure loss calculation. Starting with the general loss coefficient equation presented earlier, namely Eq. 6, the working equation after inputting air properties and unit conversions is Eq. 8 as follows.

$$\Delta P = 1.62 \times 10^{-6} K \dot{V}^2 \tag{8}$$

where the vent cap pressure drop is in inch WC and $\dot{V}$ is the airflow rate in cfm.

Total System Pressure Drop Model

Total pressure loss in a range hood ducting system from the fan outlet to the vent cap discharge to the outdoors is calculated by combining Eqs 4 through 8, depending on the type of duct, either flexible or rigid. The equations used to model and calculate the pressure loss in the range hood ducting systems are Eqs 9 and 10, with Eq.9 being for

flexible ducting systems and Eq.10 being for rigid ducting systems. The parameter L is the length of ducts in inches, and the other terms have been specified previously.

$$\Delta P = \frac{(0.0551C + 0.1635)\rho\dot{V}^2}{D^4} \cdot \frac{L}{1200} + C' \cdot \frac{\dot{V}^2}{617234} + 1.62 \times 10^{-6} K\dot{V}^2 \quad (9)$$

$$\Delta P = C_0 \cdot (cfm)^n \cdot \frac{L}{1200} + C' \cdot \frac{\dot{V}^2}{617234} + 1.62 \times 10^{-6} K\dot{V}^2 \quad (10)$$

It should be noted that the term $\frac{L}{1200}$ is based on the fact that the term is pressure drop per 100 feet, so $\frac{L}{1200}$ is the number of 100 feet intervals that the ducting system contains.

Capture Efficiency of Residential Cooking Exhaust Hoods

The purpose of the modeling efforts is to provide a tool for evaluating real-world systems, not just individual components such as fans and/or ducts acting separately, which is the limits of past models. In this regard, a capture efficiency model was investigated and with the other models presented and described previously to evaluate real world conditions for removing contaminants.

The results of tests performed by LBNL to measure capture efficiencies of range hoods were used to model pollutant capture efficiencies of range hoods in the study reported herein. All of the range hoods tested in the LBNL research were under-cabinet hoods, meaning the hoods are attached to the underside of kitchen cabinets. LBNL found that capture efficiency can be influenced by system design, burners configuration (which burner is being used), range hood type, fan setting (high, medium or low speed) and

different cooking contaminants. Unfortunately, there is no standard equation to quantify capture efficiency as a function of flow rates due to the complexity of those multiple parameters.

Therefore, in the research reported herein, the capture efficiency was modeled by using LBNL testing data, which used carbon dioxide as the tracking pollutant. In LBNL's research, three configurations were tested: both back burners, both front burners, and the oven. Capture efficiency was measured by LBNL for each configuration at each fan operating point. The fact that these LBNL experiments included only the fan and not a real-world ducting system, demonstrates the importance of the study reported here, which shows capture efficiency and pollutant removal for systems installed in actual buildings.

For both front burners and oven configurations, there appear to be no uniform trend as airflow rate goes up. In contrast for both back burner configurations, capture efficiency goes up as the airflow rate increases, so the capture efficiency in this thesis was modeled by using data measured from both back burner configurations for under-cabinet exhaust hoods. As summarized in Table 2 taken from LBNL research testing results (Delp, 2012). The CE versus cfm data from the table is plotted in Figure 7 and a trend line for all the data is also shown.

Table 2. Performance Assessment of US Residential Cooking Exhaust Hoods

Hood Category	Hood ID	Capture efficiency (CE) for various cfm						
Single grease screen	L1	cfm	94	148	200			
		CE	66	81	84			
	B1	cfm	86	119	148	179	210	
		CE	52	65	77	86	96	
Microwave	M1	cfm	147	173	280	348		
		CE	77	79	99	90		
Flat-profile	A1	cfm	86	141	198	254	309	
		CE	51	61	68	81	95	
	E1	cfm	68	120	138	176	190	222
		CE	49	68	74	78	79	81
	E2	cfm	54	80	115	178	202	229
		CE	37	50	64	77	79	85
Open capture	P1	cfm	183	210	232	252	262	
		CE	83	88	92	96	97	

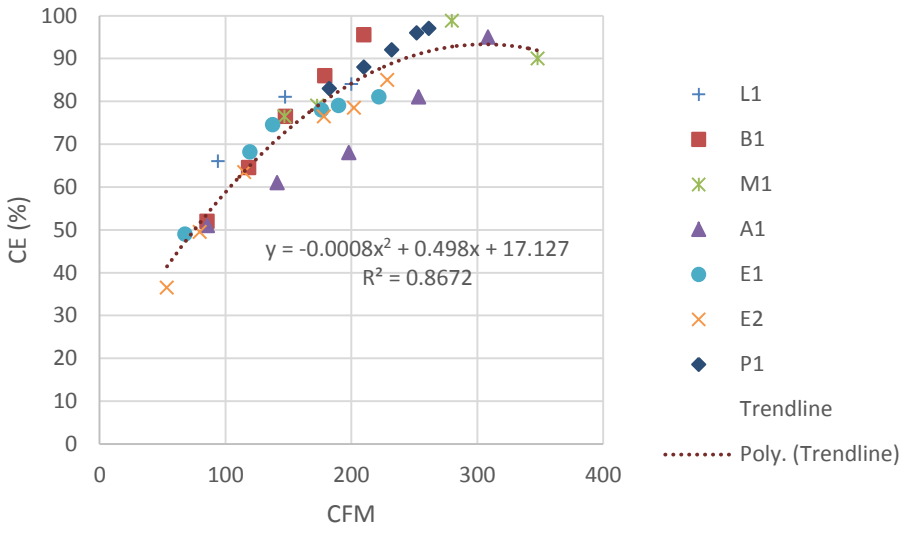

Figure 7. Capture Efficiency at Different Airflow Rates (Delp, 2012)

The CE (%) versus airflow (cfm) equation represented by the Figure 7 trend line is as follows

$$CE = -0.0008\dot{V}^2 + 0.498\dot{V} + 17.127 \quad (11)$$

Eq11 is used herein to model capture efficiency as a function of cfm for under-cabinet range hoods with both back burner configurations. The value of integrating the fan and system model with the capture efficiency model is that a designer and engineer will be able to determine actual pollutant removal based on actual flow rate, which is much different than only knowing a capture efficiency value that changes with flow rate.

CHAPTER V

TEST METHODOLOGY

This chapter focuses on the laboratory setups used to evaluate range hood performance as installed in actual world setup used in real homes for real application. As a first step, field trips were made to actual residences and discussions to have with builders. Next, a fan selected for real-world evaluation was tested in an airflow chamber setup for the purpose of obtaining the fan performance curve. Thirdly, the range hood was tested in real world system that included ducting, bends, and vent caps.

Field Trip: Present Day Range Hood Ducting System

Flexible ducting has been widely used in range hood ventilation systems due to its flexibility, which makes installation easier, and low cost; however, as society has progressed, other considerations such as aesthetics and safety are getting more attention. Given to this situation, a field trip was made to "Fall Parade of Homes" held in Bryan and College Station, Texas to research nowadays residential range hood installation strategies in order to ensure that the testing of the range hood in this study mimicked actual installed condition according to the field trip results.

It was found that, in the new houses being constructed, reasons that rigid ducts are widely used in range hood ducting systems instead of flexible ducts for safety reasons, that is to prevent grease build-up and fire hazards. In the field trip, all the houses visited were typical American style one-story houses. Discussions with house builders revealed that range hoods are usually vented through the side wall or through

the roof, with the roof plan being preferable due to aesthetics purpose. In some old apartments, flexible ducts are still used in range-hood ducting systems. Of special importance, range hood ventilation plan needs to be selected according to specific floor plans and kitchen structures. Several typical range hood ducting system were photographed and are shown in Figure 8.

(a) (b)

(c)

Figure 8. (a) Rigid Duct Vented Through Sidewall; (b) Rigid Duct Vented Through Roof; (c) Flexible Duct Vented Through Sidewall in Some Apartments

Airflow Test

The range hood was first tested on the airflow chamber setup in Riverside Energy Efficiency Laboratory (REEL) for the purpose of obtaining the fan performance curve before it was tested in the real-world system. Airflow test setup and procedures are illustrated below.

Airflow Test Setup

Airflow Chamber Specifications

Before the range hood and fan assembly was tested in a whole system, which included ducting and a vent cap, airflow tests were performed on only the range hood fan for the purpose of obtaining a fan performance curve. These tests were performed following HVI standard 916 standard procedures for testing and rating airflow, which are consistent with ANSI/AMCA 210-ANSI/ASHRAE 51standard. The range hood tested in this study was manufactured by Cyclone, it is an under-cabinet range hood and three fan speeds (high, medium and low) with a six-inch duct outlet.

These airflow tests that reflect in a fan performance curve were performed on the green airflow chamber as shown in Figure 9 located at the Riverside Energy Efficiency Laboratory (REEL). This chamber is delegated as a “Figure 12” unit, which is a technical description and delegation. This is an outlet chamber, which means that, when a fan assembly is mounted on the chamber, the chamber works as an outlet of the product, and air blows into the chamber. Usually a blower is installed at the exit of the chamber as the variable exhaust system helping adjust chamber static pressure.

Figure 9. Green Airflow Test Chamber Located at REEL

Multiple air flow nozzles are used so that they can be blocked as necessary to achieve flow measurements over a wide airflow range requirement. Nozzle board layout is shown in Figure 10, and the size, cross section area and air flow range at differential pressure limits (0.25 to 2.5 inch WC) for each nozzle are listed in Table 3.

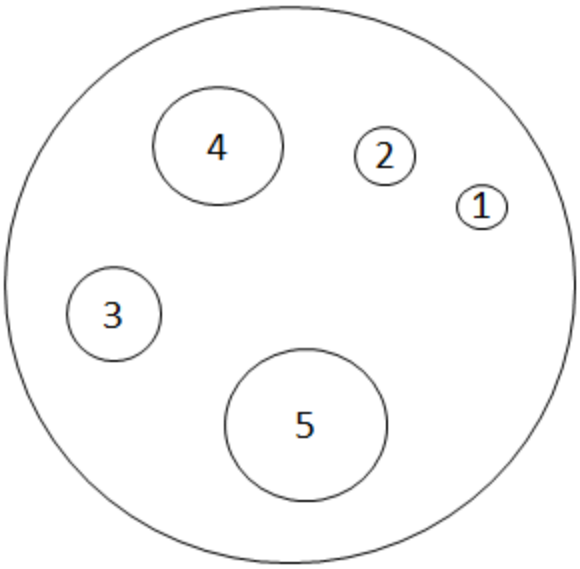

Figure 10. Nozzle Board Layout for the Green Air Flow Chamber

Table 3. Green Air Flow Chamber Nozzle Information

Nozzle Key	ISO Dia (inch)	ISO Area	Single Nozzle Flow at Differential Pressure Limits
1	0.94656	0.0048867	9.8-30.9
2	1.35216	0.0099720	19.9-63
3	3.03144	0.5012161	200.2-316.6
4	4.27476	0.0996668	398.1-629.5
5	6.75252	0.2486902	496.7-1570.8

Range Hood Mounting Description

The range hood and fan assembly prior to being tested was mounted on the chamber following specifications in HVI standard 916, The standard mounting method

for an outlet chamber and a horizontally ducted range hood is shown in Figure 11. Figure 12 presents test setup pictures, which is in accordance with the standard.

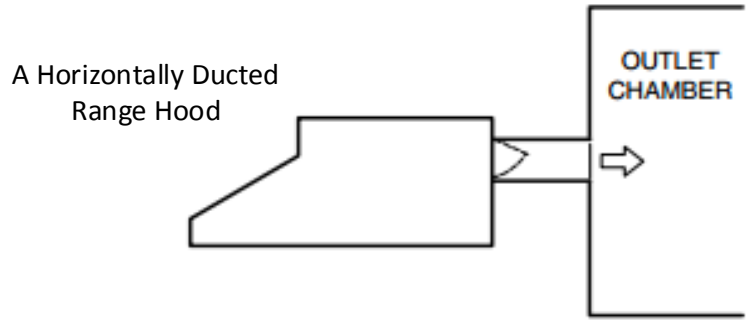

Figure 11. HVI Standard 916 Standard Test Setup for an Outlet Chamber

Figure 12. Range Hood Airflow Test Setup

A piece of reflective tape was attached to the fan blade, and a Monarch speed sensor was then used to measure rpm by exporting a signal to an ACT-3X panel tachometer that can be read by the users.

Airflow Test Procedure

The airflow test procedure used to measure data and to develop the fan curve consists of four major steps that are described below in sequence.

Step 1: Start Program, input test information and initial test note. The air and sound measurement program operation interface is shown in Figure 13, along with Figure 12 nozzle chamber green selection tab.

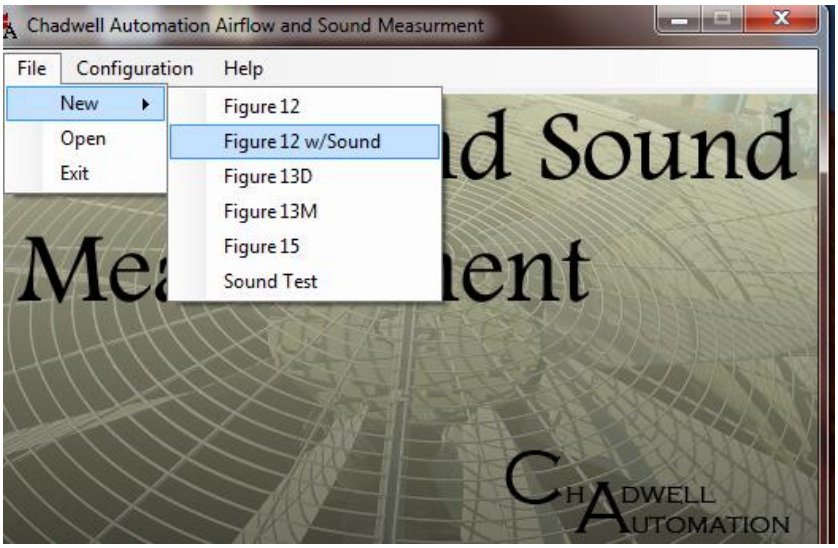

Figure 13. Airflow Test Program Operation Interface

Step 2: Prior to testing data, the pressure transducers must be zeroed as shown in Figure 14 and then checks were made to make sure that the wet bulb and dry bulb, barometric pressure are reasonable.

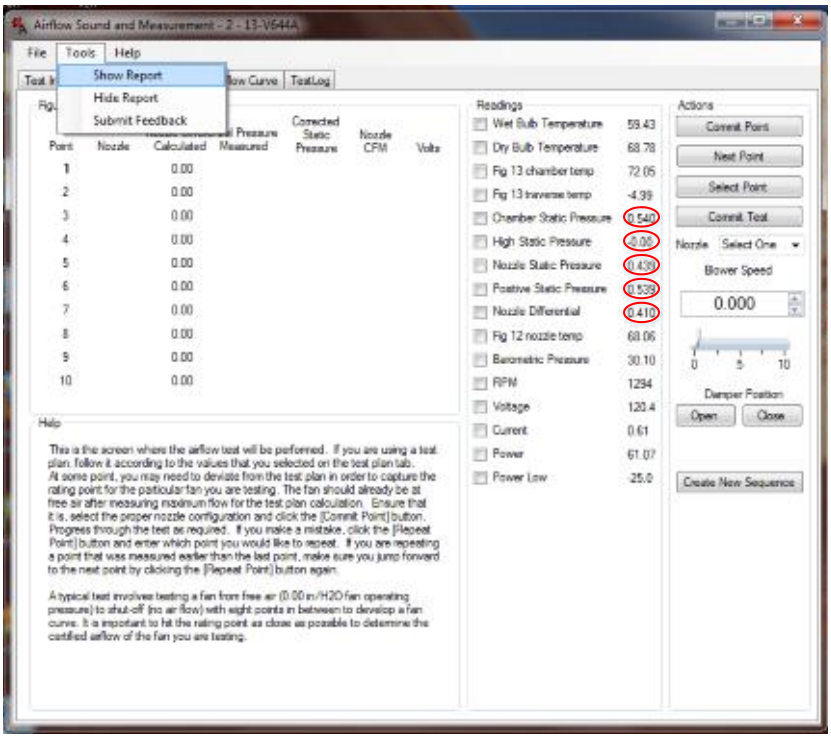

Figure 14. Zero Pressure Transducers Panel

Step 3: Fan performance curve generation.

- Select appropriate nozzle code for the appropriate chamber and nozzle configuration.
- Record the appropriate power consumption information.
- Commit a point to collect data, and then hit next point to confirm data. Ten points are committed consecutively to finish the full fan curve.

Step 4: Finish the test by export airflow reports to appropriate folders, and by taking photos of the product before removing the unit from the chamber.

Range Hood Ducting System Pressure Drop Test Setup

Tests Description and Preparation

The previous section described the test setup and procedure for developing the fan performance curve where this section does the same for a system setup consists of the range hood and fan assembly along with real-world ducting.

The range hood and system were tested in two configurations based on the field trip survey results, namely flexible and rigid ducts exiting through side walls and ceilings respectively. Specifically, the range hood was vented through the side wall via flexible ducting and rigid ducting in Case 1 and through the ceiling via rigid ducting in Case 2. In both cases, the range hood was mounted on a mobile wire shelving platform for the purpose of being moved easily by adjusting the height of each shelf as desired. The test setup was mounted horizontally along a wall in the lab based on the fact that the direction of the duct either horizontal or vertical did not impact the range hood performance. The ducts were held along the wall by using wall mounted shelves as shown in Figure 15.

Figure 15. Case 1 (Flexible Duct) Pressure Measurement Test Setup

Static Pressure Measurement

Pressure data are important parameters and were taken to follow appropriate standards and procedures. Therefore in this research, pressure is measured by using pressure taps set up in a pressure ring following ASHRAE Standard 37 (ASHRAE, 2005b), which specified dimensions for pressure taps as shown in Figure 16. For example, a tube of inner diameter D equals to ¼" was soldered to the outer plenum surface, and was centered over a hole of 1/8" drilled to form a pressure tap section. Figure 17 shows a pressure tap assembly made from a copper plate with the plates being cut into approximate 2" × 2" square pieces, and the 1" length of ¼" inner diameter copper tubing was soldered to the center of the copper piece.

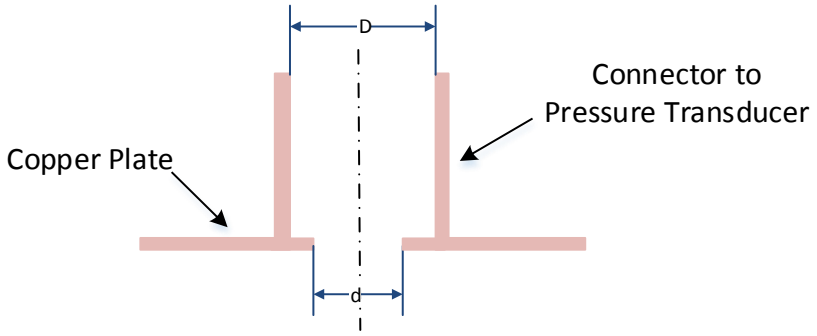

Figure 16. Pressure Tap Illustration

Figure 17. A Well Made Pressure Tap Following Standards

To complete the pressure tap assembly, for round ducts described above, four holes were drilled in the duct by using a 1/8" drill bit. The four holes are spaced equally around the circumference on the same cross section of the duct center line. The four pressure taps are then attached to the duct surface with the center line of each tube on the tap being aligned with the centerline of the holes drilled on the duct surface. The taps are

connected to each other using ½" inner diameter silicon tubing to create a pressure ring as shown in Figure 18, the purpose of the ring is to average the pressure. The blue parts are tubes.

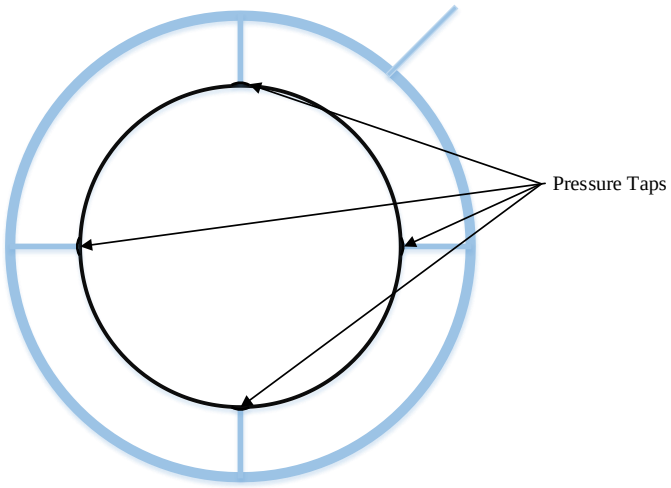

Figure 18. A Pressure Ring on a Round Duct

For the range hood and system setup, pressure needs to be measured at two positions, and the two pressure rings are labeled as follows

- P1: Range hood outlet pressure ring.
- P2: Vent cap inlet pressure ring.

P1 located at the fan outlet, is the pressure loss across the fan, which also means it is the pressure loss of the whole system, while P2 located upstream of the vent cap, is the pressure loss of the vent cap. Of special importance, the pressure loss for ducts with bends, meaning the flow region between the fan discharge and the vent cap inlet, is calculated by subtracting P2 from P1 for both Case 1 and Case 2 tests. The P1 pressure ring was on a separate circular piece of aluminum ducting, which enabled the pressure

ring remain fixed while changing ducts without attaching pressure taps to the removable ducts. The dimensions of the separate fixed pressure ring are shown in Figure 19, it can be seen that the four pressure taps located evenly around the circle surface (as described earlier and as specified by the standard), while the width of the ring is $2\frac{1}{8}$'' and diameter is 6".

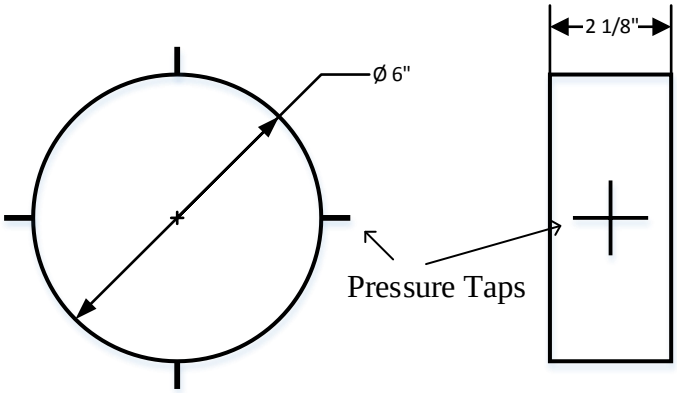

Figure 19. Dimension of the Separate Fixed Pressure Ring

To summarize, P1 is located at the outlet of the range hood to measure the pressure loss of the whole system, which is equivalent to the pressure loss across the fan. P2 is located three inches from the end of the vent cap duct, and the pressure taps are attached to the vent cap inlet using aluminum tape as shown in Figure 20. The vent cap used in the tests is a 6" round duct aluminum wall cap with damper.

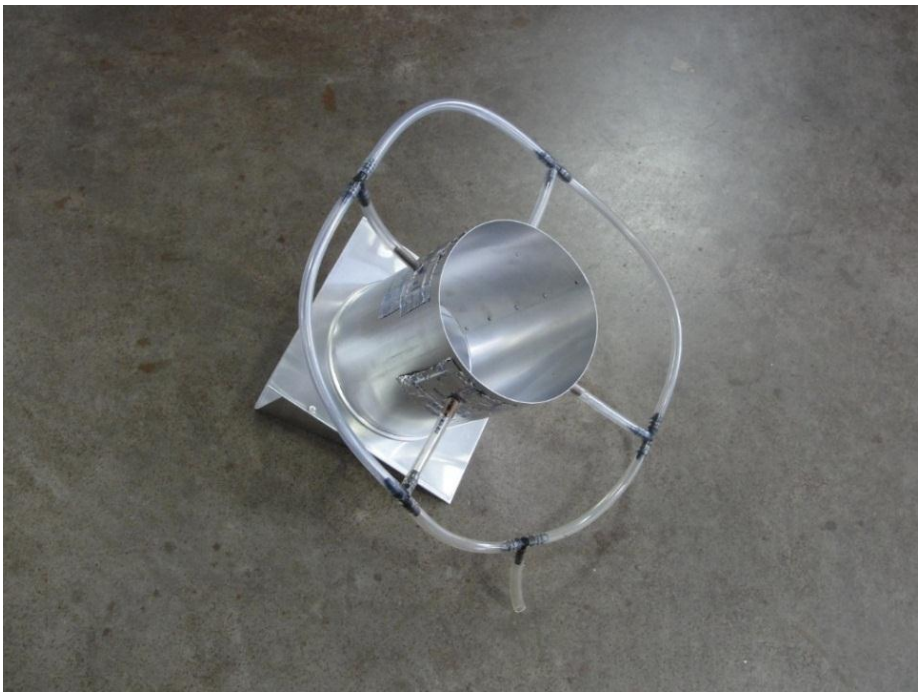

Figure 20. Pressure Ring on the Vent Cap

Case 1 Setup

The range hood and fan assembly were installed as the test setup by following all the manufacturer recommended installation heights. The most common stove top height is 36 inches, and usually a range hood is installed at a height of 26” to 32” above the cooktop following guideline suggested by manufactures for best performance. For the ceiling height, sometime between 1995 and 2004 nine-foot ceilings replaced eight-foot ceilings as the most common ceiling height in single-family homes (Borson, 2010).

The test setup dimension for flexible ducting system in Case 1 is presented in Figure 21 with the height of the cooktop being 36”, and the range hood being installed 32” above the cooktop. For flexible duct testing, three different lengths of ducts (32”, 46”, 75”) were mounted to exit a sidewall. Flexible duct lengths were measured by

laying the naturally relaxed duct on the floor and then achieved a compression ratio of about 23% compared to the fully stretched case. This compression ratio (i.e. 23%) is defined as natural compression ratio, which means that the compression ratio is measured when the flexible duct is at a natural status, without being stretched or compressed. All the flexible ducts installed in the experimental testing were with natural compression ratios. P1 as shown in Figure 21, located at the outlet of the range hood to measure the whole system pressure loss. P2 as shown located at the end of the duct length, just before the vent cap, measuring pressure drop through the vent cap. Rubber bend attachments were used to fasten the flexible ducts on the wall mounted shelve as shown in Figure 22.

The test set up for rigid ducts is presented in Figure 23, with five different lengths (32”, 46”, 75”119”, 148”) of rigid ducts being tested. In this case, P1 located one diameter (i.e. 6”) from the range hood outlet in order to avoid the turbulent flow at the outlet. It is noted that for flexible ducting tests, P1 locates exact at the range hood outlet, because the folded inner surface of flexible ducts is a main cause for turbulence, so the turbulence at the exhaust outlet can be neglected. Rigid ducts are made of galvanized steel duct, and were cut by using a sheet metal brake. Various duct lengths were connected to make longer ducts with duct tape being used at the butts to prevent leakage.

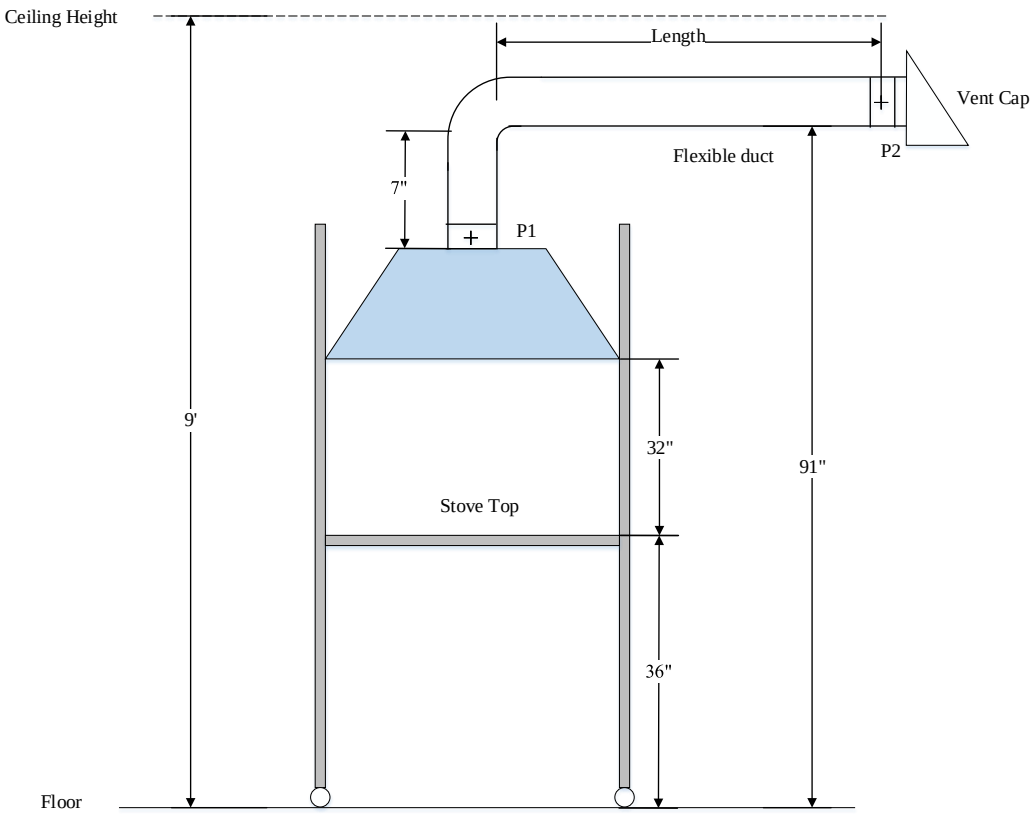

Figure 21. Case 1 Test Setup Dimension (Flexible Duct)

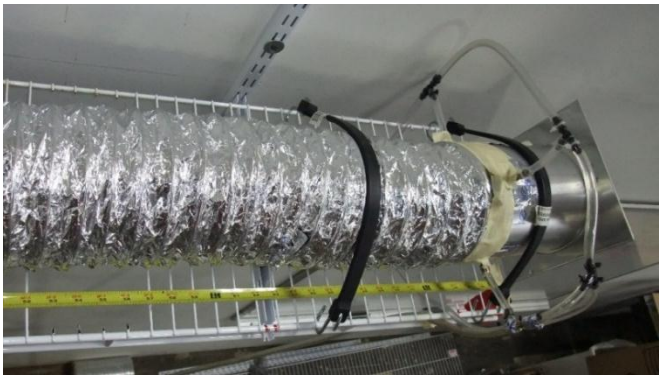

Figure 22. Flexible Duct Fastened to Shelving with a Rubber Attachment

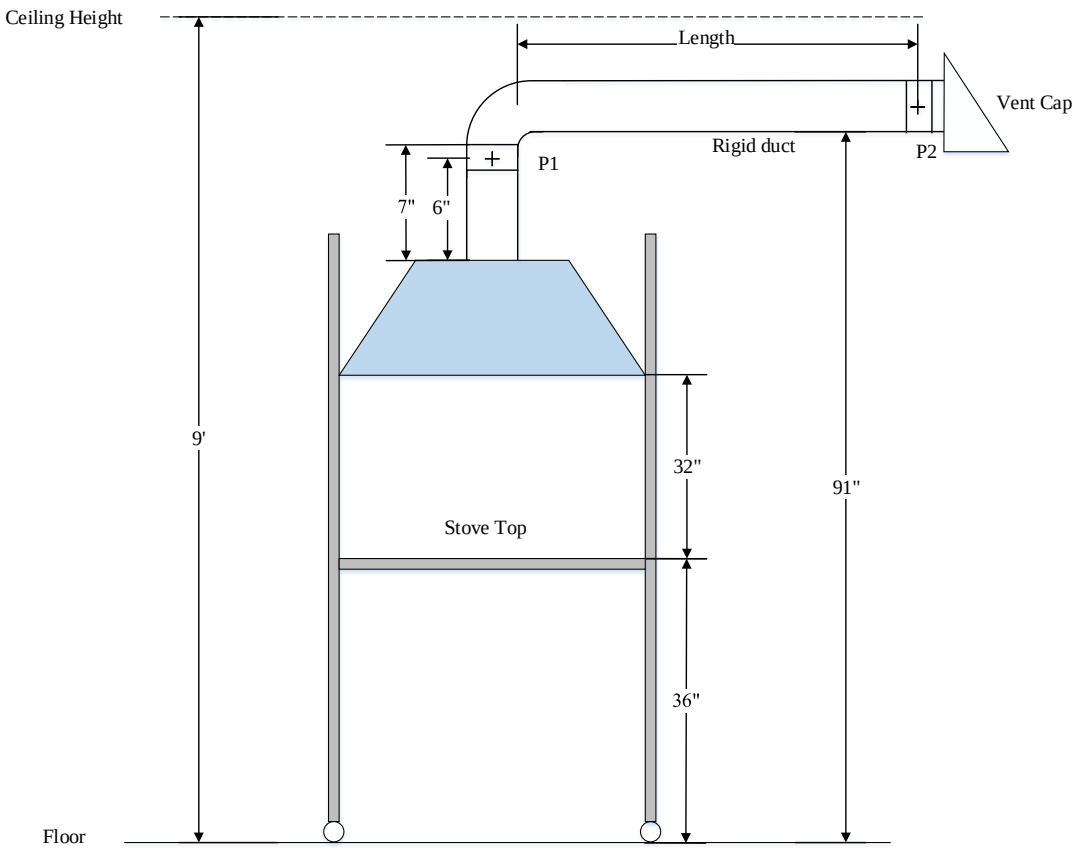

Figure 23. Case 1 (Wall Vent) Test Setup Dimension (Rigid Duct)

Case 2 Setup

The test setup for Case 2 is similar to that used in Case 1, for the rigid ducting was set up in Figure 24 with some minor differences. For example, the Case 2 setup used the same duct lengths (32”, 46”, 75”, 119”, 148”) of rigid ducts that were used in Case 1 were mounted to vent through the roof. According to the field trip, in a typical American style one-story residence, there is usually a bend above the ceiling that causes the duct to vent horizontally before venting outside instead of going straight up to the roof. In this study it is assumed that gravity will not impact range hood performance significantly,

which can be neglected. The fact that the rigid duct for the roof mount goes through the ceiling and is then directed horizontally to the outside can be seen in Figure 24. Due to the limited space in the lab and for test set up convenience. P1 located 6” from range hood outlet and in this case, the horizontal duct is 8” above the ceiling. Comparing the Case 1 wall setup in Figure 23 with the Case 2 roof setup in Figure 24, both being rigid ducts, one can observe that the Case 2 ducting length, even if the horizontal sections are of equal length for the two cases, must be longer than Case 1. The reason for this extra length is that the Case 2 roof mount ducting must reach the 9 feet high ceiling. By comparing Figure 23 and Figure 24, this extra length is determined as the difference between the distances from the floor to the horizontal duct, which is $116"\text{-}91" = 25"$.

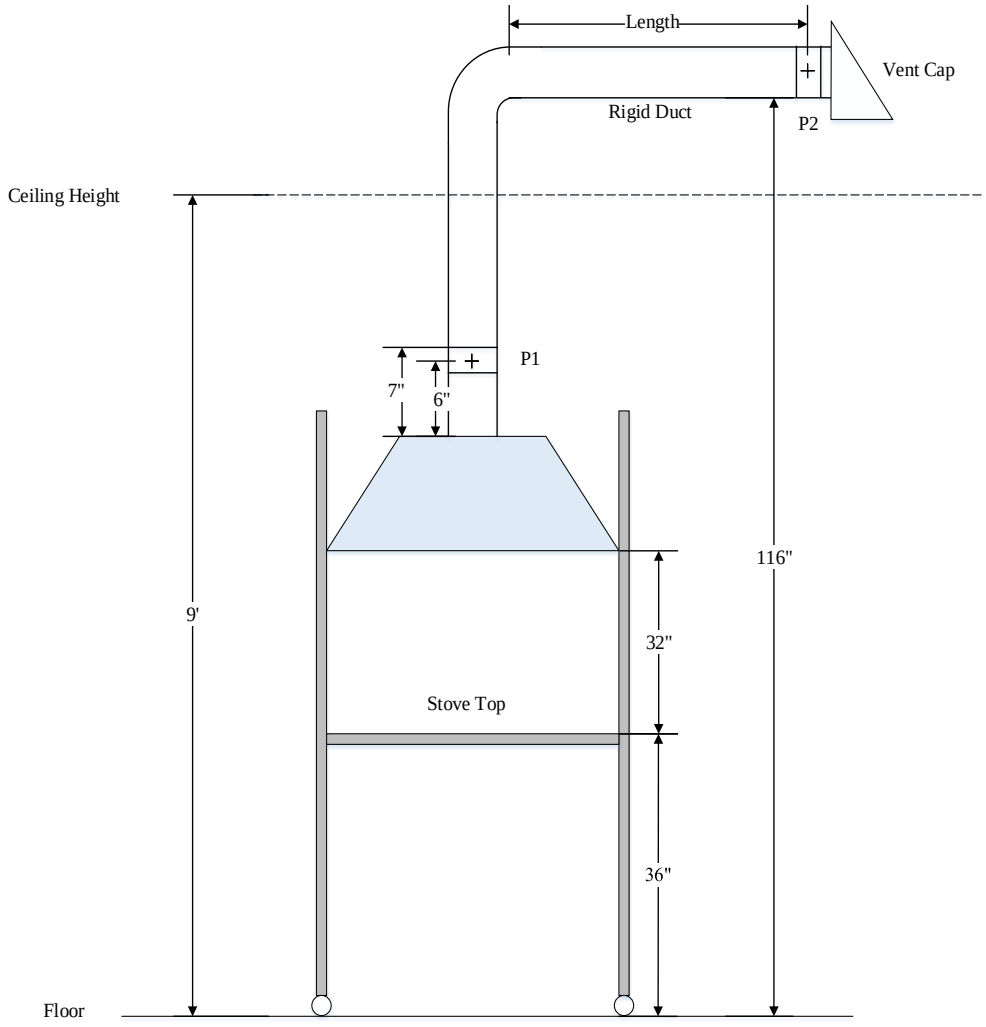

Figure 24. Case 2 (Roof Vent) Test Setup Dimension (Rigid Duct)

Data Acquisition and Instrumentation

A data acquisition (DAQ) system was used to process signals and measure data in this research. The DAQ system shown in Figure 25 consists of three parts: pressure sensors, DAQ measurement hardware, and a computer with programmable software.

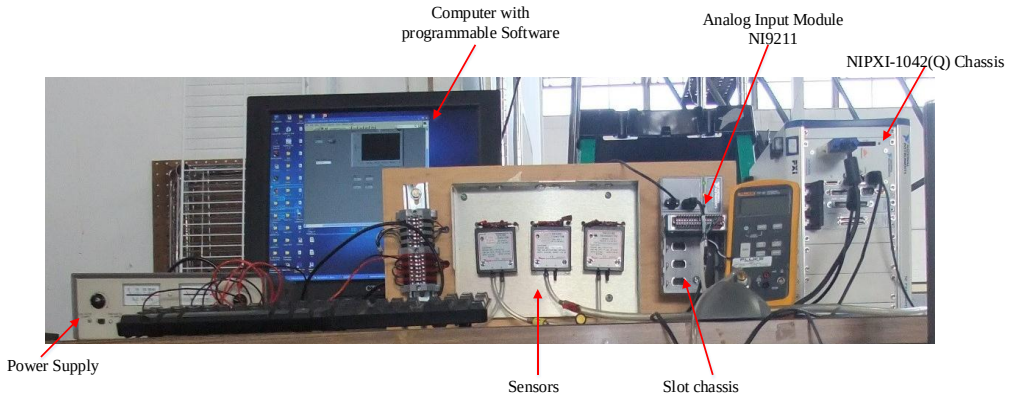

Figure 25. DAQ System

Figure 26 shows the details of the pressure sensor board, with sensor 1 and sensor 2 being used in this study and sensor 3 being used as a spare. Both of the transducers send a 4-20 mA current output signal and then a 200Ω resistor is added between the two channels on the patch board, so that the current output signal is converted to a DAQ system voltage input signal ranging from 0.8 volts to 4 volts. Table 4 lists the pressure sensor specifications while Figure 27 shows the sensor wiring diagrams. As shown in Figure 27 the sensors are connected to the NI9205 spring terminal connector, which is a 32-channel single-ended analog input module with a signal amplifier built-in made by National Instrument. The NI9205 is inserted to a 4-slot USB chassis with the model being cDAQ-9174 made by National Instruments. The chassis is connected to NI PXI-1042(Q) 8-slot PXI chassis with the chassis working as a main frame. The computer uses the voltage signal sent from DAQ board and transfers it to a pressure value by using a linear calculation.

Table 4. Detailed Information of the Sensors

Sensors	Manfr.	Model	Supply	Range(in H2O)	%Accuracy(+/-FS)	Drift	Output
ΔP	Dwyer	616-1	10-35VDC	0-3.0	0.25%	.5%FS/yr	4-20mA DC
ΔP	Dwyer	616-1	10-35VDC	0-3.0	0.25%	.5%FS/yr	4-20mA DC

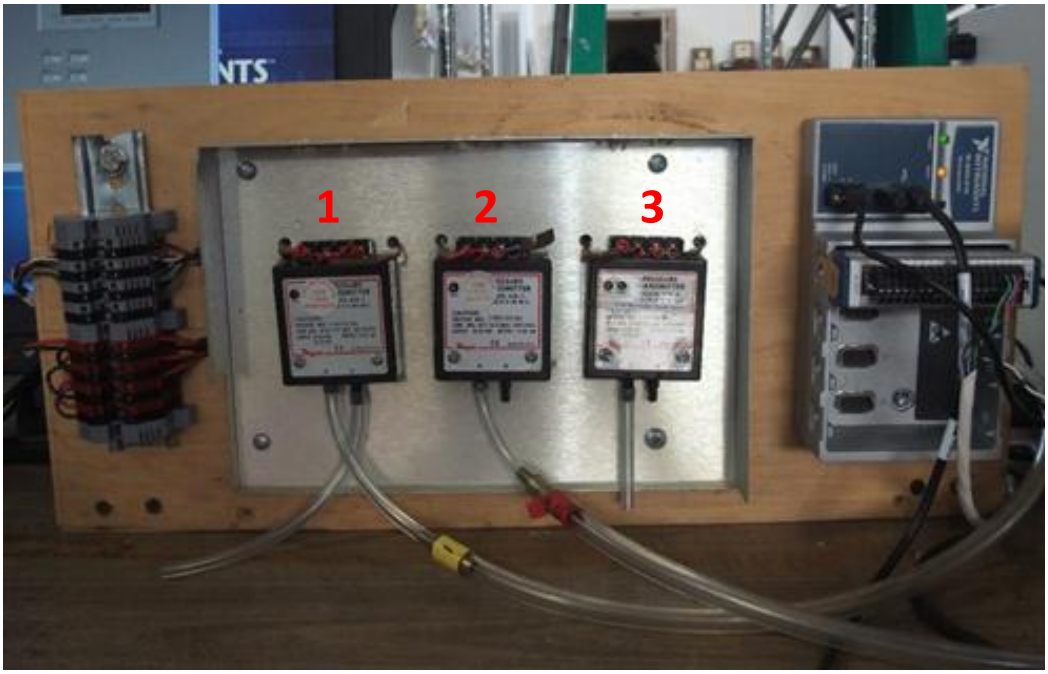

Figure 26. Pressure Sensor Board

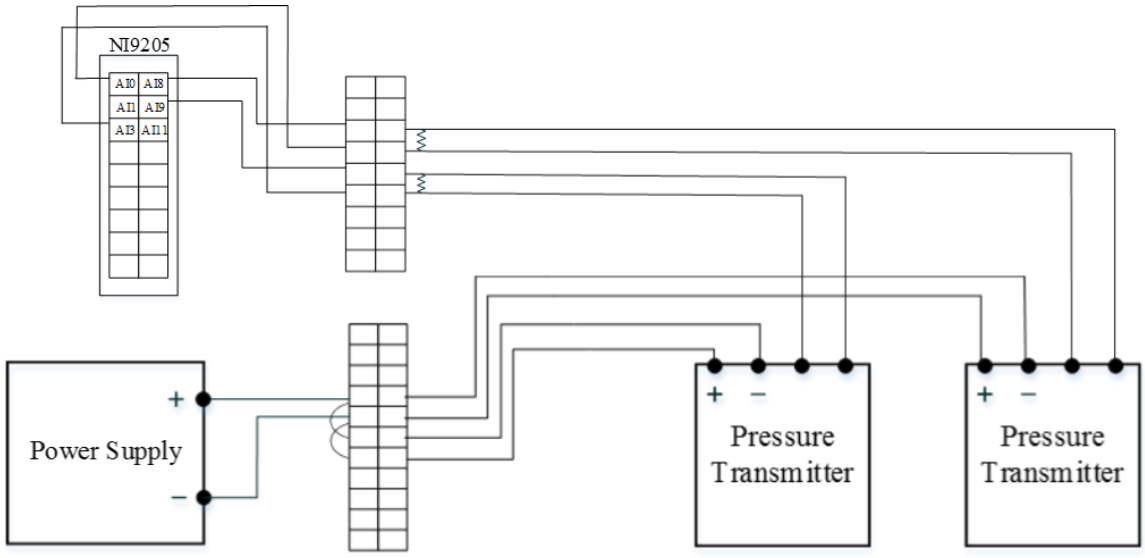

Figure 27. Sensors Wiring Diagram

LabVIEW was used to acquire data during all testing. Because LabVIEW programs are called virtual instruments (VIs), meaning they use graphical languages for programming. Figure 28 shows the LabVIEW VI front panel with indicators added to the front panel to show graph and report measurements of both the voltage and pressure. After the front panel window is created, graphical source code is added in the block diagram window to control the front panel with Figure 29 showing the block diagram

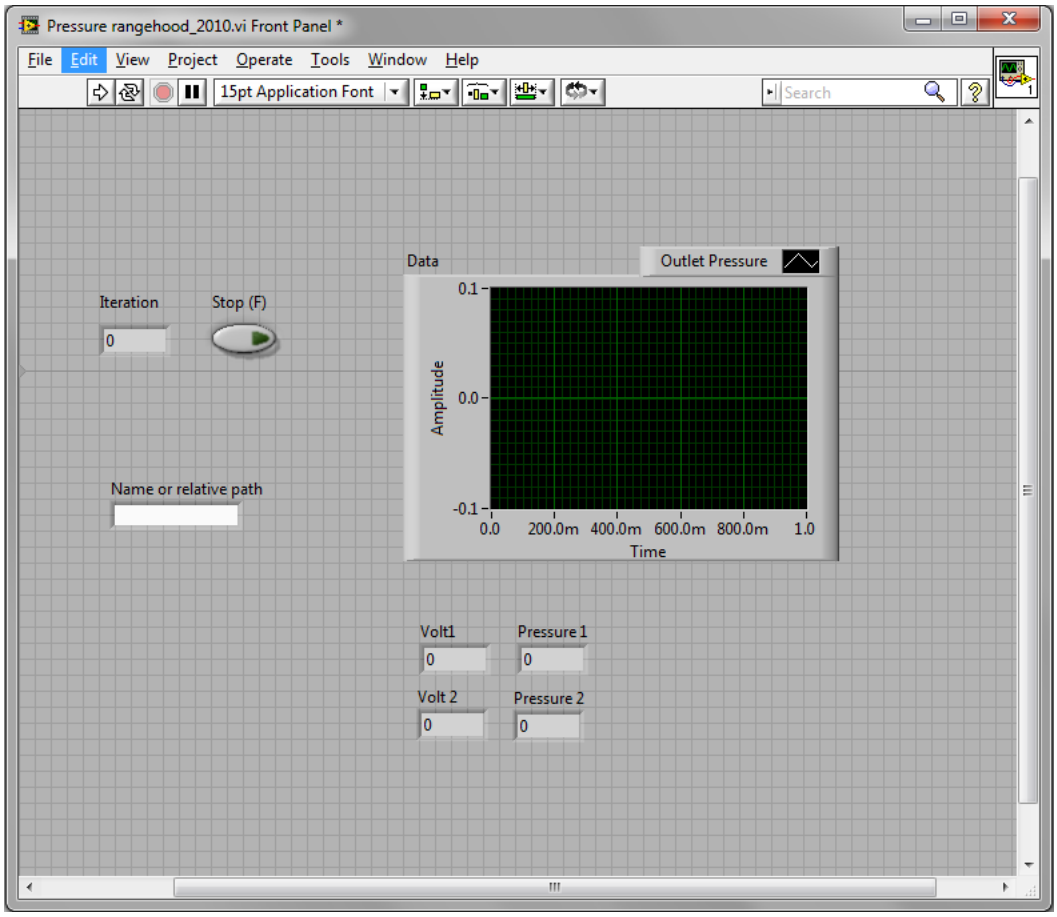

Figure 28. LabVIEW Program Front Panel

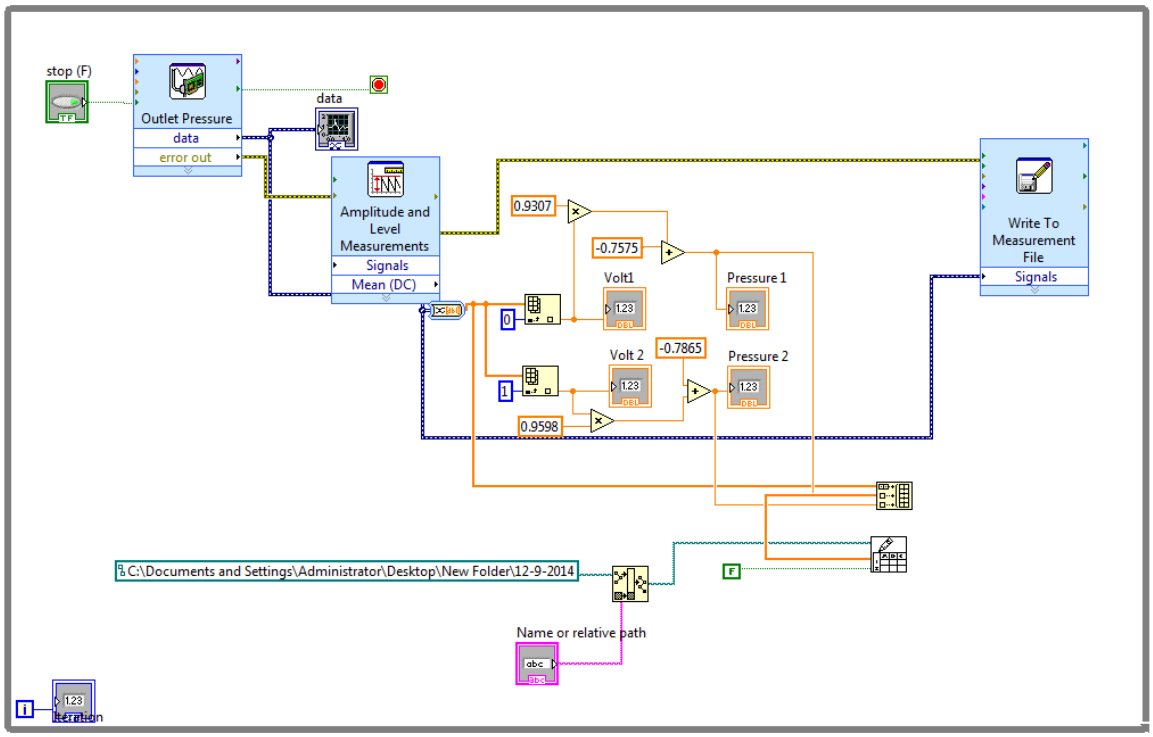

Figure 29. Block Diagram in LabVIEW Program

Test Procedure

Step 1: First, set up the test, including installing the correct duct to the right duct length.

Step 2: Start the range hood and let it run for at least 30 minutes.

Step 3: Boot up the DAQ PC, and LabVIEW, open the program.

Step 4: Calibrate the sensors at the beginning of each test period. The detail of pressure sensor calibration is present in Abstract C.

Step 5: Zero the P1 and P2 pressure transducers.

Step 6: Start the test, when the iterations reach 20, press stop button. The data will be saved automatically to the target folder.

Step 7: Measure the rpm manually using Monarch PLT200, which is a digital optical tachometer, write down the rpm every one second, in total 20 times.

Step 8: Substitute data to the mathematical model built previously and analyze the data.

CHAPTER VI

RESULTS AND DATA ANALYSIS

Separate experimental tests were performed to obtain the fan performance curves, which utilized the air flow test setup, and to obtain the system performance curves, which used the range hood and ducting system setup. Once the above data measurements were performed, then a detailed analysis of the data and test results was done.

Airflow Tests and Fan Curves

Figure 30 shows the range-hood fan performance curves obtained from airflow tests and data taken at three different fan speeds. The experimental curves shown in Figure 30 follow typical fan performance curve trends thus verifying the reliability of the tests.

Figure 31 shows the RPM versus airflow rate measured data for each fan speed, and a number of conclusions can be drawn based on Figure 31 observations. For example, we can tell that as the static pressure goes up then the air flow rate decreases and the rpm increases. This phenomena can be explained by the fact that as static pressure goes up, there is more flow resistance, which results in a smaller airflow rate, and then the rpm goes up to compensate for the impact caused by the decrease in airflow rate.

The fan curves in Figure 30 will later be used for generating system curves and operating points, while Figure 31 will later be used to calculate airflow rates during the

system analysis.

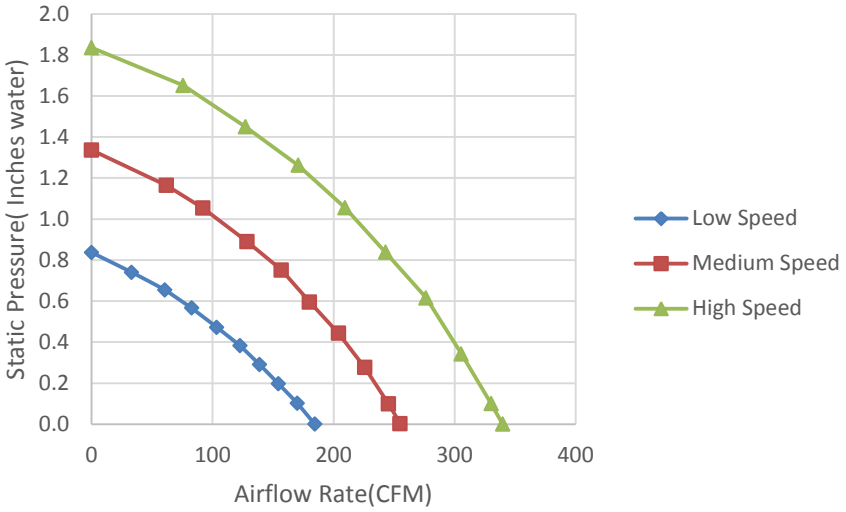

Figure 30. Measured Fan Performance Curves at Different Fan Speeds

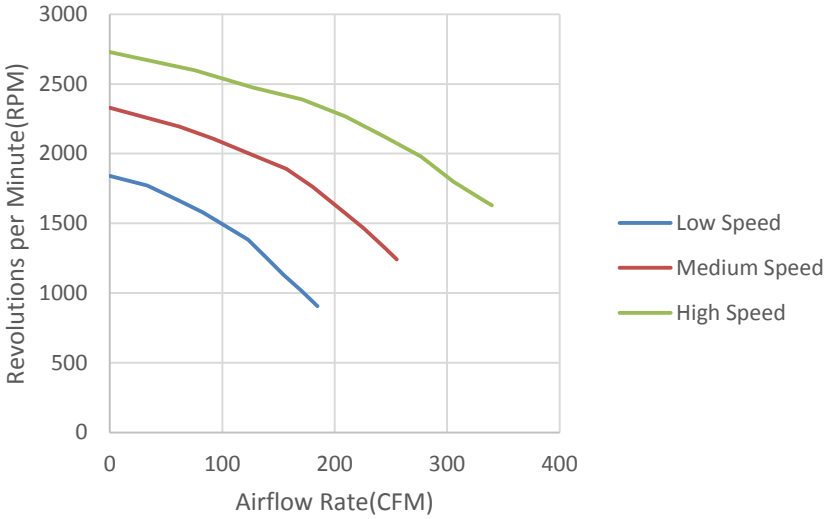

Figure 31. Measured RPM versus Airflow Rate at Different Fan Speeds

System Curves and Operating Points

The fan curves obtained from the pressure drop and flow rate data in the previous section did not consider the system, meaning the ducts and bends that it might eventually be attached to. In the system tests that were performed in the previous section, the fan was integrated into a ducting system that resulted in a unique pressure drop and flow rate, otherwise called the operating point.

Test Results for Case 1 and Case 2

Experiments were performed on the Case 1 and Case 2, namely the wall-mounted and roof mounted exhausts respectively, by using the test system and test procedures described in detail in an earlier section. Specifically, test results for Case 1 and Case 2, including measured pressure loss through the system (P1), measured pressure loss through the vent cap component (P2), measured pressure loss through the duct with bend component (P1-P2), and the rotation speeds, which was used to find airflow rates are presented in Table 5 and Table 6 for Case1 and Case 2, respectively. Additional explanation is appropriate to explain how airflow rates are obtained by using linear interpolations on RPM versus airflow rate curves. For every test, the rpm was recorded a total of twenty times at one second intervals, and then averaged as the representative fan speed for each test. Linear interpolations were then applied to calculate the airflow rate by using Figure 31 presented earlier.

Table 5. Test Results for Case 1 (Sidewall Vent Cap)

Duct Type	Duct Length (inch)	Speed	P1 (inch WC)	P2 (inch WC)	P1-P2 (inch WC)	Rotational Speed(rpm)	Airflow rate(cfm)
Rigid Duct	32	High	0.393	0.329	0.064	1865.25	295.103
		Medium	0.235	0.195	0.040	1439.45	229.132
		Low	0.123	0.105	0.018	1065.1	163.569
	46	High	0.376	0.302	0.074	1844.5	298.426
		Medium	0.223	0.178	0.045	1417.1	232.122
		Low	0.118	0.096	0.022	1052.85	165.282
	75	High	0.355	0.254	0.101	1835.6	299.85
		Medium	0.214	0.152	0.062	1415.6	232.323
		Low	0.118	0.081	0.037	1046.15	166.218
	119	High	0.376	0.246	0.130	1832.6	300.331
		Medium	0.230	0.153	0.077	1415	232.403
		Low	0.122	0.083	0.039	1047.25	166.064
	148	High	0.396	0.253	0.143	1852.7	297.113
		Medium	0.240	0.153	0.087	1437.5	229.393
		Low	0.134	0.085	0.049	1067	163.303
Flexible Duct	32	High	0.627	0.172	0.455	2030.24	265.047
		Medium	0.378	0.107	0.271	1581.43	207.383
		Low	0.202	0.061	0.141	1172.57	149.228
	46	High	0.669	0.146	0.523	2052.17	259.995
		Medium	0.393	0.092	0.301	1591.33	206.318
		Low	0.208	0.054	0.154	1177.14	148.663
	75	High	0.700	0.106	0.594	2068.77	256.172
		Medium	0.426	0.066	0.360	1613.89	202.838
		Low	0.227	0.038	0.189	1187.21	147.420

Table 6. Test Results for Case 2 (Through Roof Vent Cap)

Duct Type	Duct Length (inch)	Speed	P1(inch WC)	P2(inch WC)	P1-P2 (inch WC)	Rotational Speed (rpm)	Airflow rate(cfm)
Rigid Duct	32	High	0.359	0.270	0.089	1821.9	302.044
		Medium	0.215	0.161	0.054	1409.1	233.192
		Low	0.119	0.089	0.030	1043.5	166.589
	46	High	0.360	0.260	0.100	1830.9	300.603
		Medium	0.215	0.155	0.060	1410.45	233.012

Table 6. Continued

Duct Type	Duct Length (inch)	Speed	P1(inch WC)	P2(inch WC)	P1-P2 (inch WC)	Rotational Speed (rpm)	Airflow rate(cfm)
Rigid Duct	46	Low	0.116	0.085	0.031	1048.7	165.862
	75	High	0.377	0.253	0.124	1844.6	298.890
		Medium	0.228	0.153	0.075	1428.75	230.563
		Low	0.127	0.086	0.041	1057.65	164.611
	119	High	0.389	0.240	0.149	1841.6	298.890
		Medium	0.230	0.142	0.088	1422.3	231.426
		Low	0.130	0.080	0.050	1049.55	165.743
	148	High	0.406	0.239	0.167	1868.05	294.927
		Medium	0.243	0.143	0.100	1442.5	228.188
		Low	0.132	0.079	0.053	1071	162.604

Predicted Pressure Loss for Case 1 and Case 2

The predicted pressure losses through individual components of the tested range hood ventilation system were obtained by using the mathematical models developed in Chapter IV. Pressure losses through flexible ducts and rigid ducts were calculated by using Eq.4 and Eq. 5, respectively. Of special importance, the equations need to be multiplied by L/1200 in order to obtain pressure loss through the whole duct length because L is in inches and the pressure loss calculation is for 100 feet of ducting. Pressure loss through bends in flexible ducts or rigid ducts can be predicted by using Eq.7, with different loss coefficients for the two types of ducts being used. Finally Eq.8 can be used to predict pressure losses across the vent cap component. To obtain the total pressure loss through the whole system, either simply sum up the pressure loss through individual components (i.e. ducting, bends and vent caps) or use Eq.9 and Eq.10 for flexible and rigid duct range hood systems, respectively. Predicted pressure loss results

for Case 1(flexible and rigid ducts) and Case 2 (rigid ducts) are presented in Table 7, Table 8 and Table 9. The pressure drops (loss) in these three tables are listed as follows,

P1 Predicted pressure loss through the whole system

P2 Predicted pressure loss through the vent cap

P1-P2 Predicted pressure loss through the duct with bend part

P3 Predicted pressure loss through the duct

P4 Predicted pressure loss through the bend

along with airflow rates.

Table 7. Predicted Pressure Loss for Case 1 (Flexible Ducts)

Duct Length (inch)	Fan Speed	Airflow rate(cfm)	P1(inch WC)	P2(inch WC)	P1-P2 (inch WC)	P3(inch WC)	P4(inch WC)
32	H	265.047	0.588	0.168	0.420	0.192	0.228
	M	207.383	0.360	0.103	0.257	0.118	0.139
	L	149.228	0.186	0.053	0.133	0.061	0.072
46	H	259.995	0.633	0.162	0.470	0.251	0.219
	M	206.318	0.398	0.102	0.296	0.158	0.138
	L	148.663	0.207	0.530	0.154	0.082	0.072
75	H	256.172	0.748	0.157	0.590	0.378	0.213
	M	202.838	0.469	0.099	0.370	0.237	0.133
	L	147.420	0.248	0.052	0.195	0.125	0.070

Table 8. Predicted Pressure Loss for Case 1 (Rigid Ducts)

Duct Length (inch)	Fan Speed	Airflow rate(cfm)	P1(inch WC)	P2(inch WC)	P1-P2 (inch WC)	P3(inch WC)	P4(inch WC)
32	H	295.103	0.276	0.209	0.067	0.019	0.048
	M	229.132	0.167	0.126	0.041	0.012	0.029

Table 8. Continued

Duct Length (inch)	Fan Speed	Airflow rate(cfm)	P1(inch WC)	P2(inch WC)	P1-P2 (inch WC)	P3(inch WC)	P4(inch WC)
32	L	163.569	0.085	0.064	0.021	0.003	0.015
46	H	298.426	0.289	0.214	0.076	0.027	0.049
	M	232.122	0.176	0.129	0.046	0.017	0.030
	L	165.282	0.089	0.065	0.024	0.009	0.015
75	H	299.85	0.307	0.216	0.091	0.041	0.050
	M	232.323	0.185	0.129	0.056	0.026	0.030
	L	166.218	0.095	0.066	0.029	0.014	0.015
119	H	300.331	0.330	0.216	0.114	0.064	0.050
	M	232.403	0.200	0.129	0.070	0.040	0.030
	L	166.064	0.103	0.066	0.037	0.021	0.015
148	H	297.113	0.337	0.211	0.126	0.077	0.049
	M	229.393	0.203	0.126	0.077	0.048	0.029
	L	163.303	0.104	0.064	0.040	0.026	0.015

Table 9. Predicted Pressure Loss for Case 2 (Rigid Ducts)

Duct Length (inch)	Fan Speed	Airflow rate(cfm)	P1(inch WC)	P2(inch WC)	P1-P2 (inch WC)	P3(inch WC)	P4(inch WC)
32	H	302.044	0.302	0.219	0.083	0.033	0.050
	M	233.192	0.181	0.130	0.05	0.020	0.030
	L	166.589	0.093	0.067	0.027	0.011	0.015
46	H	300.603	0.306	0.217	0.089	0.040	0.050
	M	233.012	0.185	0.130	0.055	0.025	0.030
	L	165.862	0.094	0.066	0.028	0.013	0.015
75	H	298.890	0.316	0.214	0.103	0.054	0.049
	M	230.563	0.190	0.127	0.063	0.033	0.029
	L	164.611	0.098	0.065	0.033	0.018	0.015
119	H	298.89	0.339	0.214	0.125	0.076	0.049
	M	231.426	0.205	0.128	0.077	0.047	0.030
	L	165.743	0.107	0.066	0.041	0.026	0.015
148	H	294.927	0.344	0.208	0.136	0.088	0.048
	M	228.188	0.210	0.125	0.084	0.055	0.029
	L	162.604	0.108	0.064	0.044	0.030	0.015

Comparison between System Curves for Case 1 and Case 2

In this section, Case 1 and Case 2 results for predicted and actual system curves are compared and analyzed. Specifically, Figure 32, Figure 33 and Figure 34 compare system curves for Case 1 (flexible ducts), Case 1 (rigid ducts) and Case 2 (rigid ducts), respectively. All solid lines stand for predictions, and dashed lines stand for the actual situation based on experimental data. From these figures, it can be observed that for all cases both predicted and actual pressure losses increase as the duct lengths are increased. Also, pressure losses in the flexible duct system changes more than those in the rigid duct systems as duct lengths increase. For example, comparing 75" and 32" duct lengths for flexible and rigid ducts at high fan speeds, the flexible duct length is 2.34 times longer while the pressure loss is 12.72 times higher. In contrast for rigid ducts, when the duct length is increased by the same amount, then the pressure loss is only increased by 1.11 times.

Additional analysis of the results in Figure 32 through 34 reveal that, for the flexible duct system, there is no uniform comparison trend over all flow rates as flexible duct lengths get longer. For example, when flexible duct lengths are equal to 46", then the predicted system curve almost overlaps with the actual system curve, while at duct lengths less than 46", then the predicted pressure loss is lower than the actual pressure loss. Finally, as flexible duct lengths are increased beyond 46", the predicted pressure loss is higher than the measured pressure loss.

In contrast to the comparison for the flexible duct situation, predicted pressure drop system curves are always lower than actual system curves for all rigid duct lengths

at each fan speed. This comparison for the rigid duct systems means that pressure losses in the real situation are always higher than those predicted by the model.

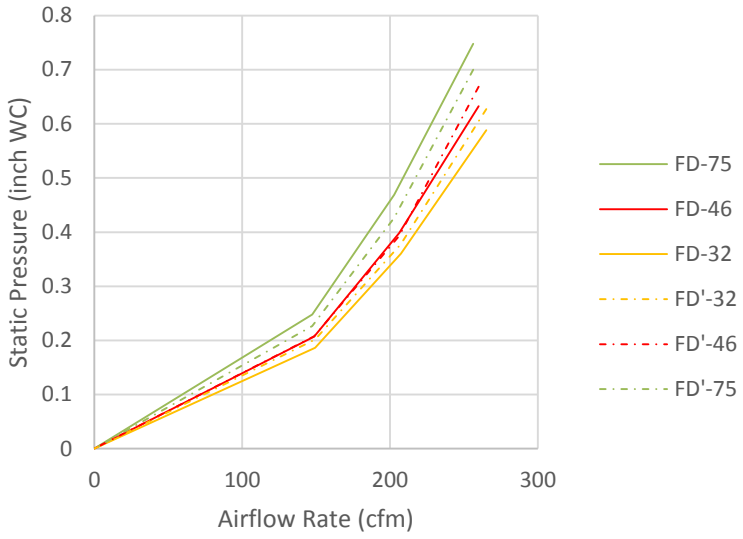

Figure 32. Comparison between System Curves for Case 1 (Flexible Ducts)

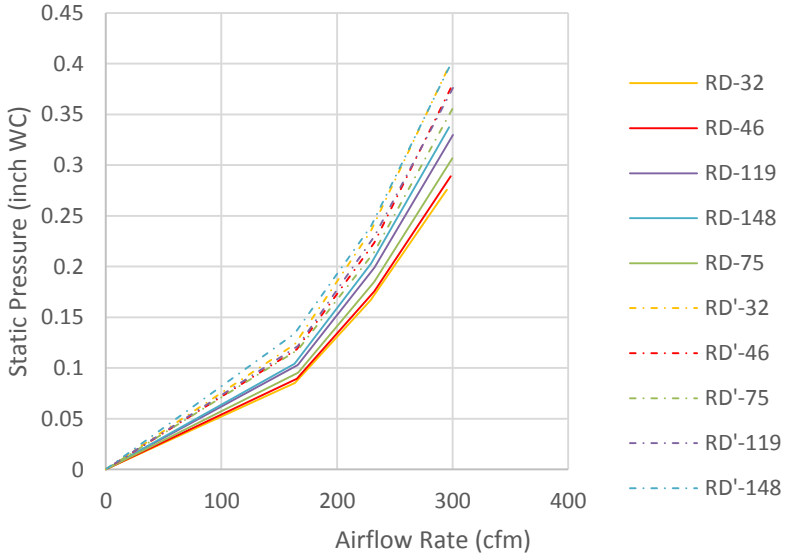

Figure 33. Comparison between System Curves for Case 1 (Rigid Ducts)

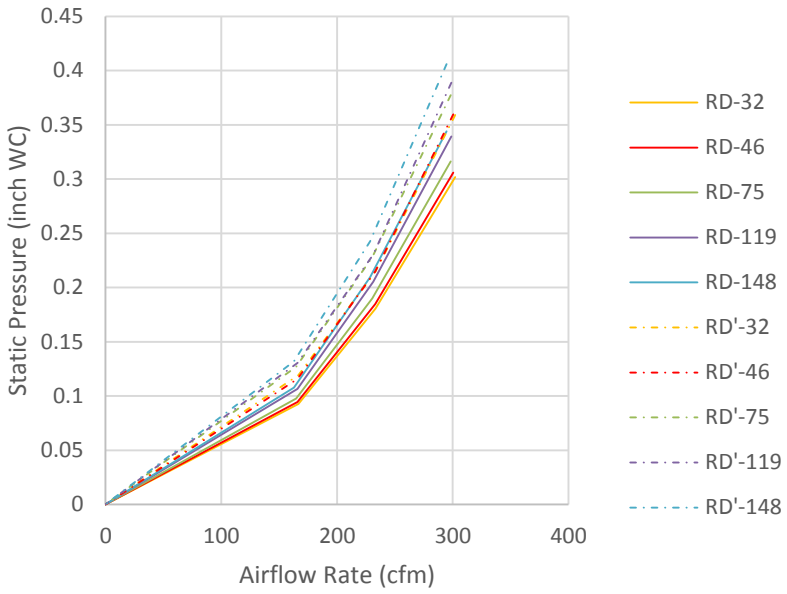

Figure 34. Comparison between System Curves for Case 2 (Rigid Ducts)

Comparison between Operating Points for Case1 and Case 2

Predicted operating points and actual operating points for all cases are compared in this section. The operating points are determined by plotting fan curves and system curves together with the intersection point being the operating point. Actual and predicted operating points for the flexible-duct ventilation systems are plotted and compared in Figure 35. It can be observed that similar to previous system curve comparison for flexible ducts, there is no uniform trend for operating points. The predicted operating points can be higher or lower than actual operating points depending on the flexible duct length.

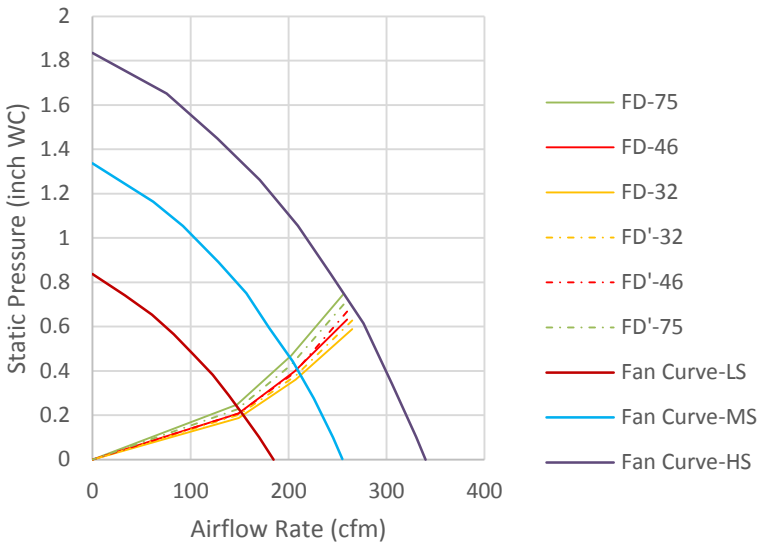

Figure 35. Comparison between Operating Points for Case 1 (Flexible Ducts)

Predicted and actual operating points for Case 1 and Case 2 rigid duct ventilation systems are compared in Figure 36 and Figure 37. As can be seen in these figures, rigid duct system curves and operating points for different duct lengths are close to each other. Selecting the 75" duct length for analysis, operating points at low and medium fan speeds for the 75" rigid duct length are plotted in Figure 38 and Figure 39 for Case 1 and Case 2, respectively. In both cases, the predicted operating points are lower than the actual operating points, which means that in actual real-world systems, the static pressure values predicted for design are higher and the airflow rates are lower. It can also be observed that for a given flow rate (e.g. 200cfm) the pressure drop is slightly higher for Case 2, which is to be expected because it has a longer overall duct length compared to Case 1.

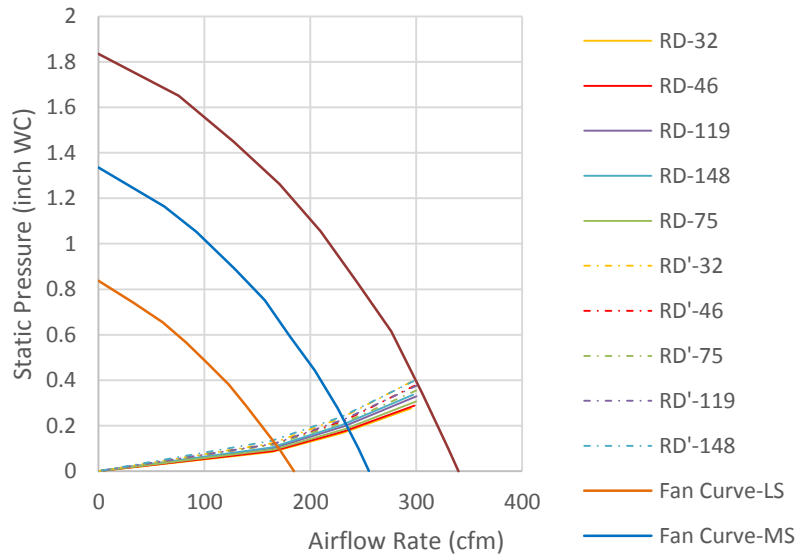

Figure 36. Comparison between Operating Points for Case 1 (Rigid Ducts)

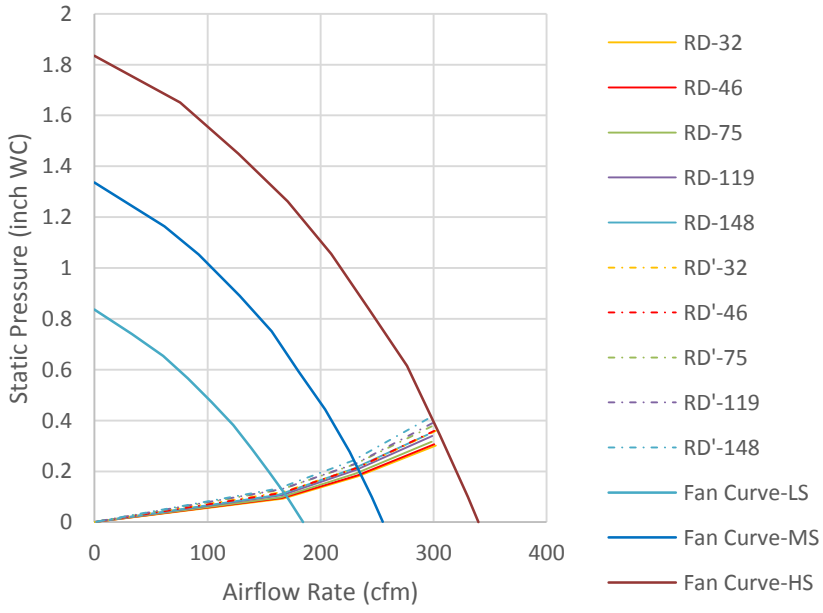

Figure 37. Comparison between Operating Points for Case 2 (Rigid Ducts)

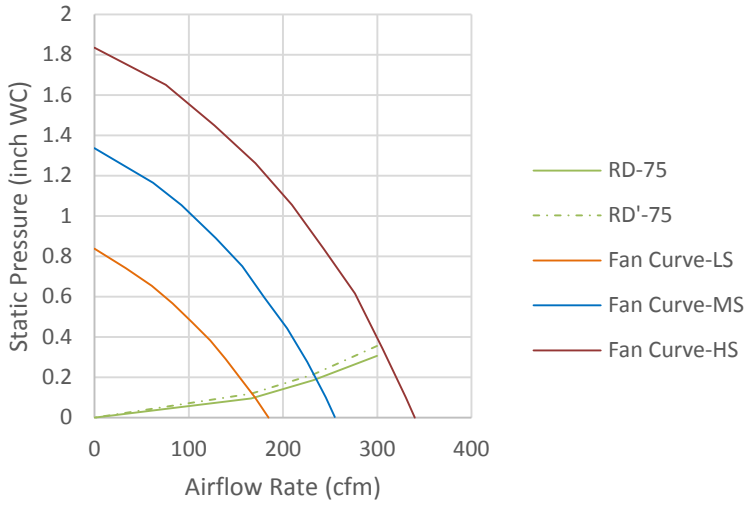

Figure 38. Comparison between Operating Points for 75" Duct Length in Case 1 (Rigid Duct)

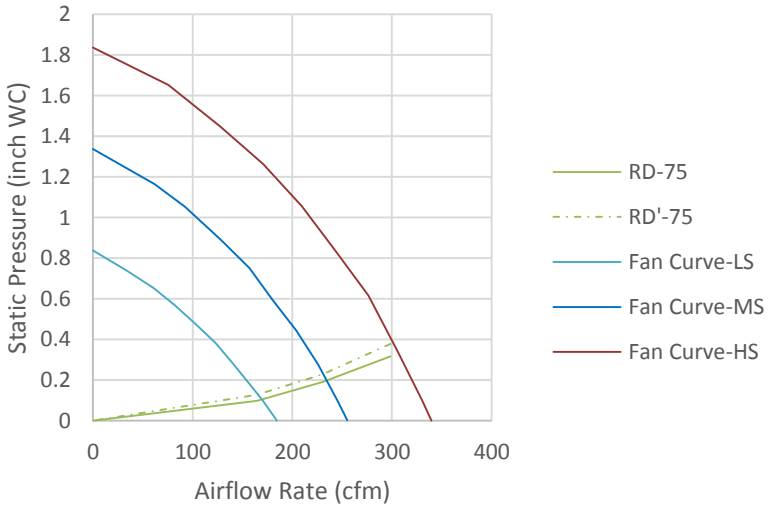

Figure 39. Comparison between Operating Points for 75" Duct Length in Case 2 (Rigid Duct)

Operating points for the two wall-mounted vent cap systems in Case 1 and Case 2, which differ in their use of flexible and rigid ducts, are compared by plotting fan and system curves in Figure 40. It can be observed that the Case 1 flexible duct has an

operating point that has a lower flow rate and higher pressure compared to Case 2, the rigid duct which has a higher flow rate and lower pressure.

The x and y values of operating points for all cases are listed in Table 10, where y is the static pressure in inch WC and x is the airflow rate in cfm. The percentage difference shown is the difference between the actual value and the predicted value divided by the actual value and then converted to a percentage (multiplied by 100). A positive percentage means the actual value is larger than the predicted value, while a negative percentage means the opposite. We can see that the percentage difference for flexible ducts is higher than that of rigid ducts, which means that the mathematical model for rigid-duct ventilation system is able to make design predictions more accurately than the mathematical model for flexible ducts.

It can be observed that in Table 10 that predicted and actual values for flexible ducts are close, ranging from 3% to 13% differences, even though there are no uniform trends for flexible duct system operating points. The predicted and actual rigid duct system can also be compared by using the results in Table 10. For the rigid-duct system, x and y values in both cases at each fan speed do not show much difference between predicted and actual values. For example, taking an average of the x and y values from both cases at low fan speeds, the predicted air flow rate is 0.9% higher than the actual flow rate, and the predicted static pressure is 6% lower than actual value. At the medium fan speed, the predicted air flow rate is 0.5% higher than the actual value, while the predicted static pressure is 8% lower than the actual one. Nearly all of the percentage differences are less than 10%, which indicates that the mathematical model is adequate

for predicting pressure drops and flow rates (i.e. operating points) in flexible and rigid ducting range hood ventilation systems, considering the fact that in the real-world other parameters may have uncertainties of 10% or more.

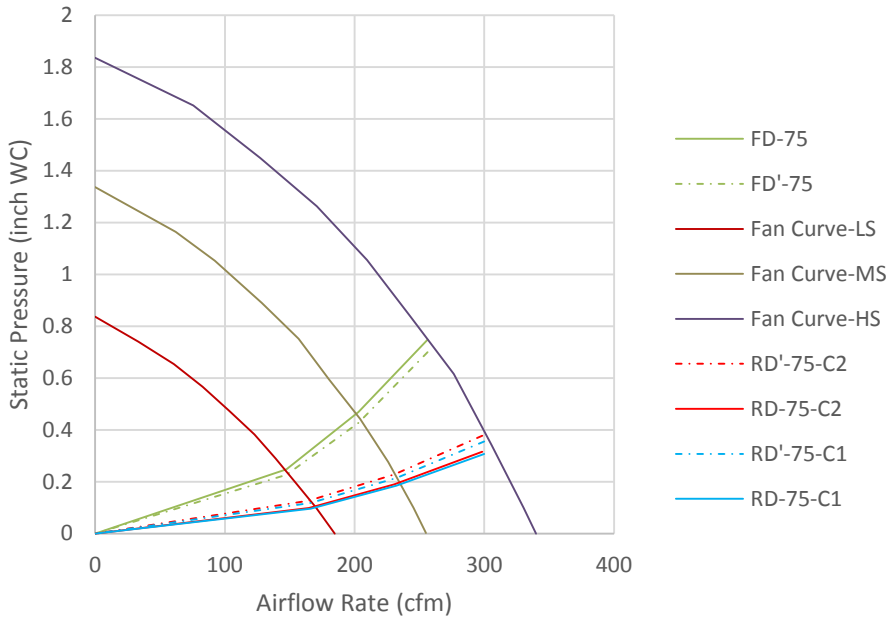

Figure 40. Comparison of Operating Points for Case 1 and Case 2

Table 10. x and y Value of Operating Points for Each Case

Cases		Case 1 (Flex duct)		Case 1 (Rigid duct)		Case 2 (Rigid duct)	
Coordinates		x(cfm)	y(inch WC)	x(cfm)	y(inch WC)	x(cfm)	y(inch WC)
Low fan speed	Real	150	0.22	168.5	0.13	168	0.12
	Predicted	145	0.23	170	0.12	170	0.11
	Difference percentage	3.3%	-4.6%	-0.9%	4.2%	-1.0%	8.1%
Medium fan speed	Real	205	0.43	231	0.21	230	0.22
	Predicted	200	0.48	232	0.20	231	0.20
	Difference percentage	2.4%	-12.9%	-0.4%	7.1%	-0.7%	9.1%

Impact Analysis

Nomenclature are introduced for a clear understanding. In the impact analysis, several new terms, including, ducting component (duct and bend combined), vent cap component and total system. They are similar to previous terms such as duct part, vent cap and whole system used in previous sections, yet they are slightly different in some cases more descriptive.

In this section, pressure drops both predicted and actual are compared and analyzed for major system components, namely the vent cap component and the ducting component (duct and bend combined) and for the total system, which is the summation of the two major components. Selecting the 75" duct length for analysis, the predicted and actual pressure losses through the vent cap component, ducting component and the total system for Case 1 are shown in Figure 41 and Figure 42 for flexible and rigid ducts, respectively. Solid lines stand for predicted and the dashed lines stand for the actual situation. The pressure loss comparisons for the other duct lengths are present in Appendix E.

Analyzing the curves in Figure 41 and Figure 42 shows that for the flexible duct system, the ducting component is more influential than the vent cap on the range-hood system performance, which means that the total system pressure drop mainly comes from the pressure drop of the flexible ducting component. In contrast, for the rigid-duct system, the vent-cap component has a stronger impact than the rigid duct on the total system pressure drop, which also explains why the pressure drop through the rigid ducting component does not change much as the duct gets longer. The impacts of the

individual components in Case 2 are compared to the component impacts in Case 1(rigid duct) in Figure 43. Again the vent cap component is more influential than the rigid ducting component.

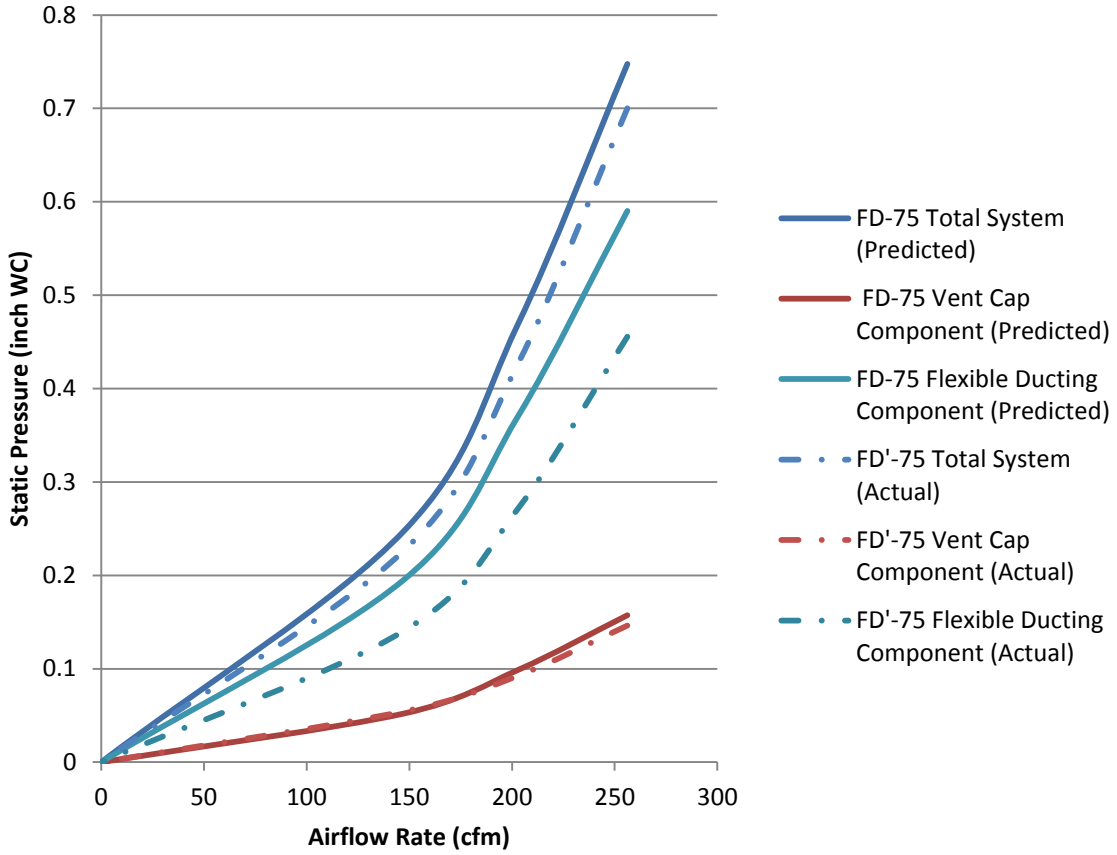

Figure 41. Actual and Predicted Pressure Loss for Components and Total System for 75" Duct Length in Case 1 (Flexible Duct)

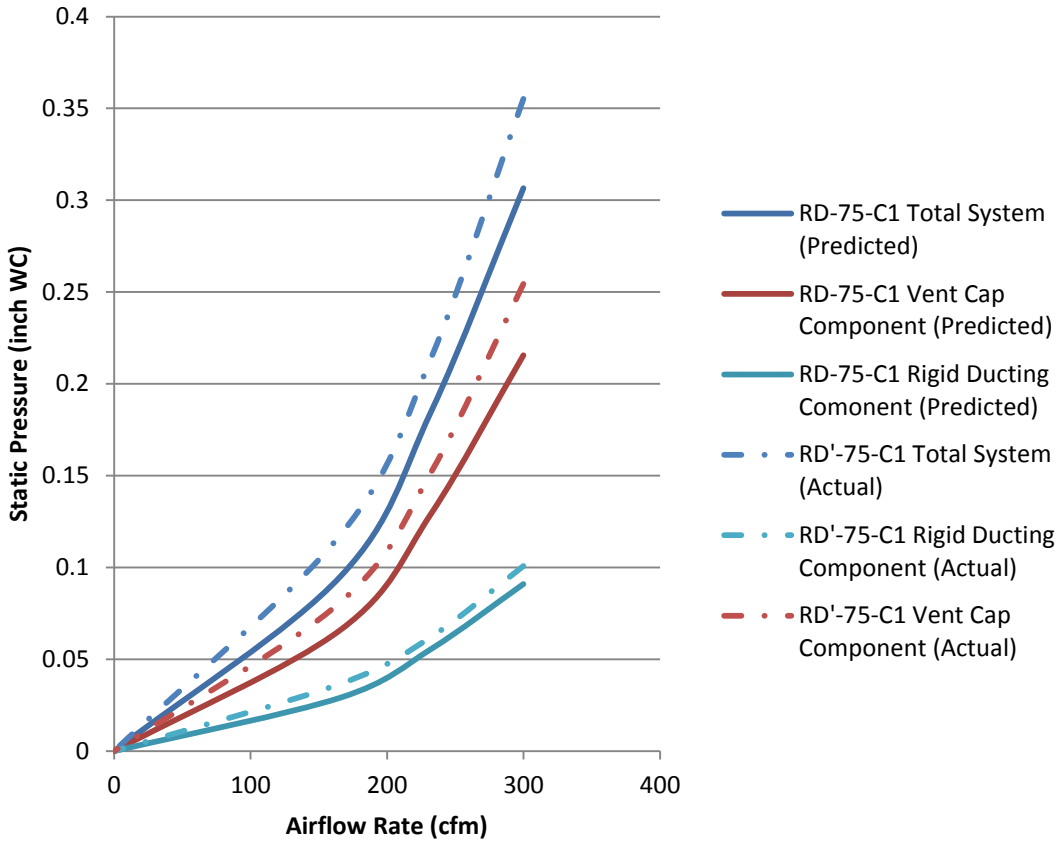

Figure 42. Actual and Predicted Pressure Loss for Components and Total System for 75" Duct Length in Case 1 (Rigid Duct)

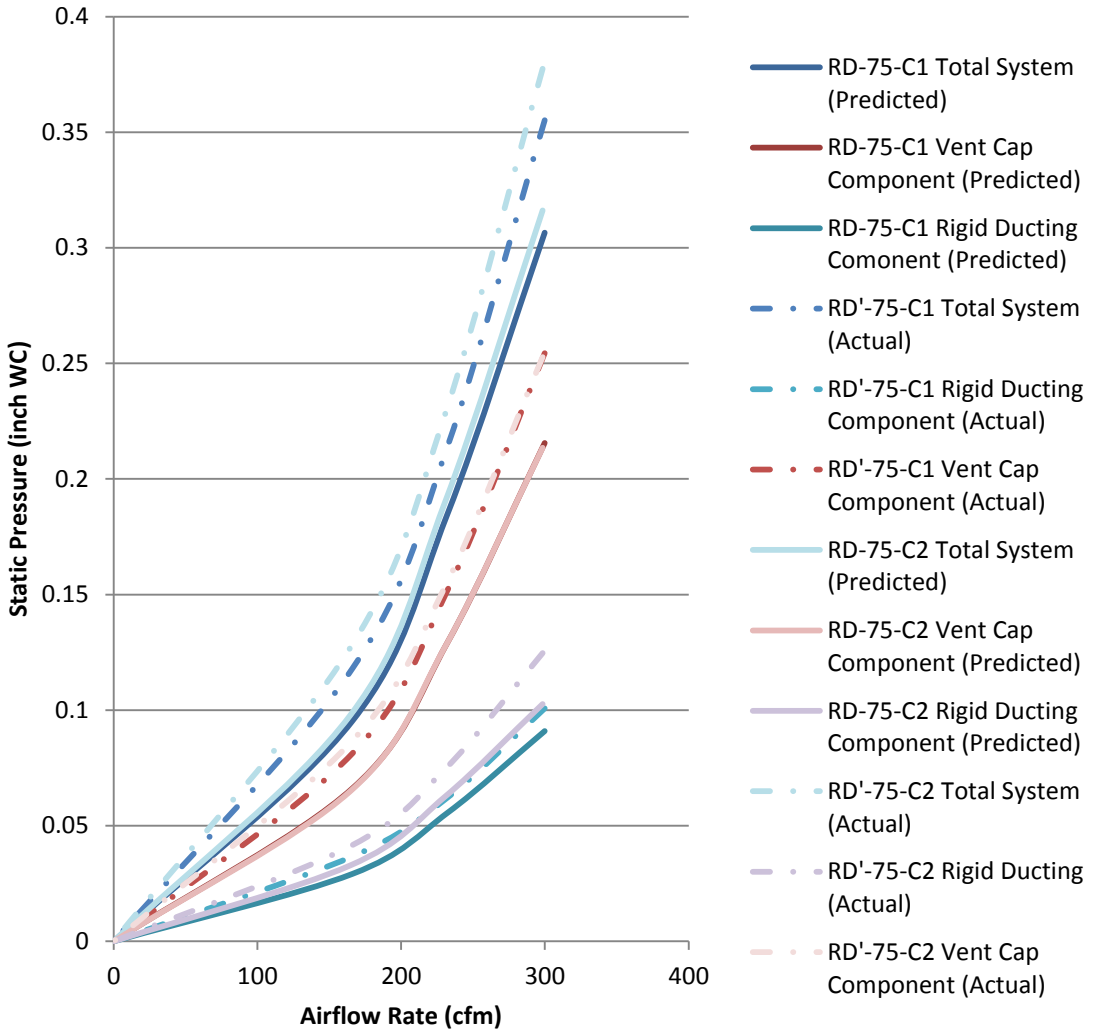

Figure 43. Comparison of Individual Component Impact Between Case 1 and Case 2

Capture Efficiency

The capture efficiency equation, namely Eq.11 as a function of range-hood flow rate was developed previously by utilizing experimental data in the literature. Because experiments have been performed in this thesis project to obtain operating points from actual fan and system curves, one can now determine capture efficiency for actual

operating systems. Therefore the capture efficiency results for Case 1 and Case 2 at operating points are presented in Table 11 and Table 12, respectively

Table 11. Capture Efficiency for Case 1

Duct Length and Fan Speed	Capture Efficiency for Case 1 (%)							
	Flexible Duct			Rigid Duct				
Duct Length (inch)	32	46	75	32	46	75	119	148
High	93	93	92	94	94	95	95	94
Medium	86	86	85	89	90	90	90	89
Low	74	73	73	77	78	78	78	77

Table 12. Capture Efficiency for Case 2

Duct Length and Fan Speed	Capture Efficiency for Case 2 (%)				
	Rigid Duct				
Duct Length (inch)	32	46	75	119	148
High	95	95	95	95	94
Medium	90	90	89	90	89
Low	78	78	77	78	77

The capture efficiencies in Table 1for Case 1 flexible ducts are plotted in Figure 44, while capture efficiencies for rigid ducts in Case 1 and Case 2 are plotted together in Figure 45.

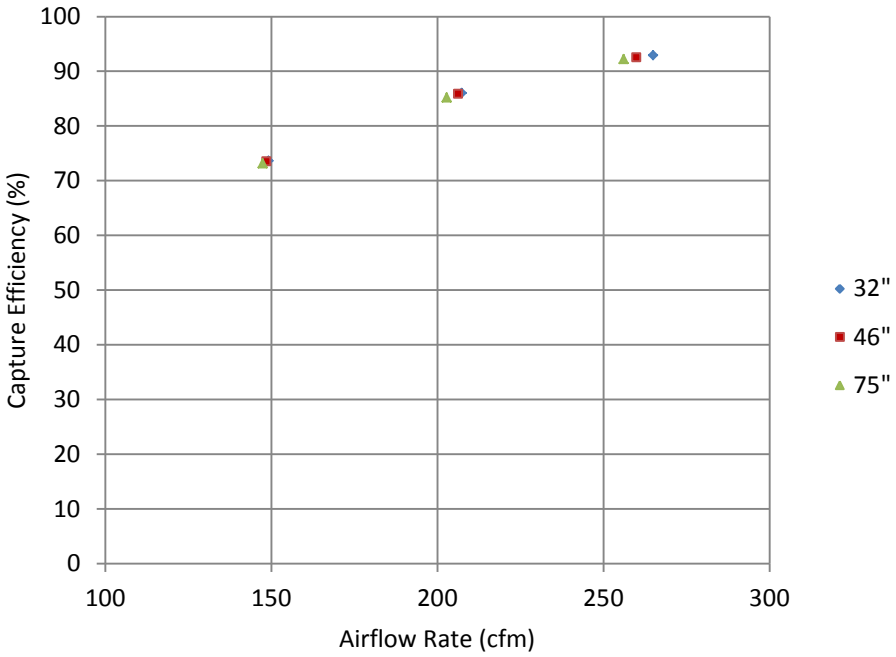

Figure 44. Capture Efficiency for Flexible Ducts (Case 1)

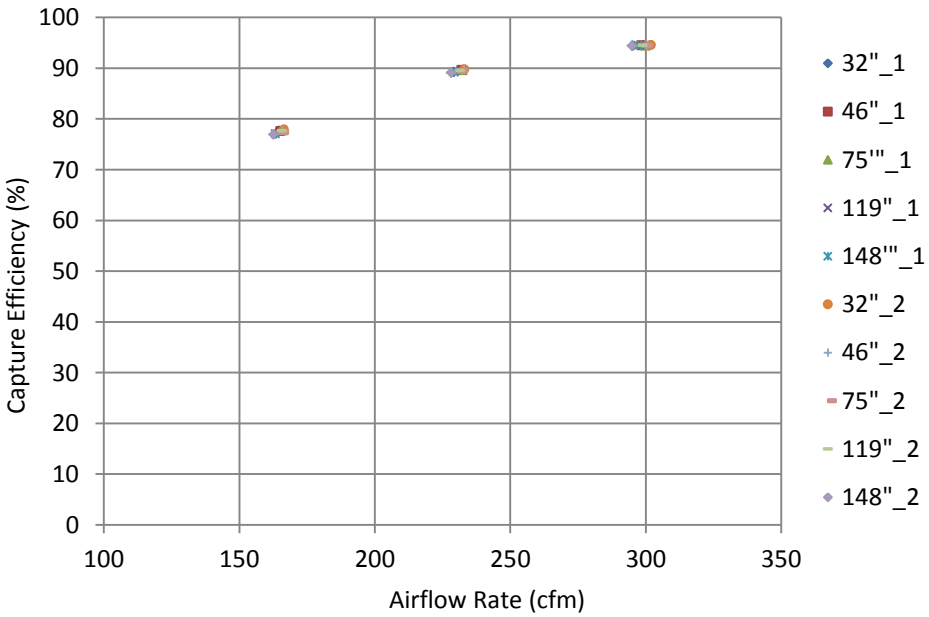

Figure 45. Capture Efficiency for Rigid Ducts (Case 2)

An analysis of the capture efficiency results for actual operating points presented in Table 11 and Table 12, along with results in Figure 44 and Figure 45, provides significant insight into how range-hood systems should be designed to remove contaminants. Observations of both figures show that capture efficiency for both flexible ducts and rigid ducts at the same fan speed even overlap for different duct lengths. To summarize, it would appear that for the fan and system setup, the capture efficiency is mainly a function of fan speed.

The comparison of capture efficiencies between flexible ducts and rigid ducts is shown in Figure 46. Capture efficiencies for rigid-duct ventilation systems are higher than that of flexible-duct systems by about 5.4% when working at the same fan speed.

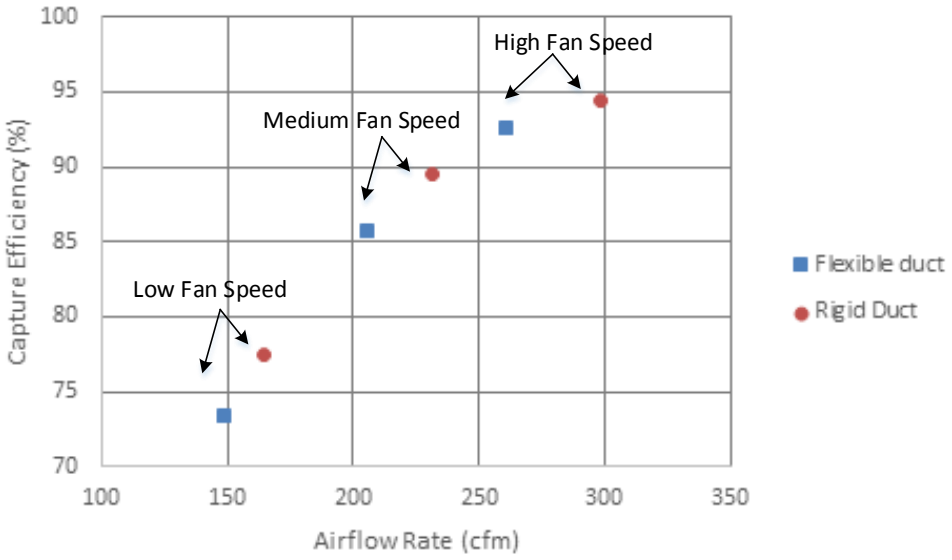

Figure 46. Comparison of Capture Efficiency between Flexible and Rigid Ducts

CHAPTER VII

CONCLUSIONS

The purpose of this study is to evaluate the performance of range-hood fans in real systems that include ducts and vent caps. The basis for this performance evaluation of real systems is a series of experiments performed to obtain a fan curve and also to evaluate a range-hood and fan assembly connected to a variety of ducting systems that are representative of what is found in actual homes. In addition, mathematical models were developed to predict range-hood ventilation system performances. The predicted values and the measured results were compared to perform an analysis and assessment of real world range hood operations and to provide a design tool for the future. Finally the real-world data in this study produced flow rates for actual fans and ducting systems, which means that for the first time that laboratory measured capture efficiencies as a function of flow rates could now be applied to real-world situations.

Comparisons of predicted and measured results show that for rigid ducts at all lengths for all situations, the predicted system pressure losses are lower than measured pressure losses. With regard to operating points at low fan speeds, the predicted air flow rates are about 1% higher than the flow rates for actual situations, while the predicted static pressure is lower than the actual situation by about 6%. For the operating point at a high fan speed, the predicted air flow rate is 0.5% higher than actual flow rate, while the predicted static pressure is lower than the actual one by 8.1%. All the differences between predicted and actual data for rigid ducts are less than 10%, which means that

the mathematical model developed for rigid-duct range hood ventilation can successfully and can predict the range hood system performance.

For flexible ducts, the trends between predicted and test results are not uniform in that predicted pressure losses can be higher or lower than measured results depending on the length of the flexible duct. In terms of predicted and actual operating points, the percent pressure difference can be as large as 13%, while flow rate differences are about 3%.

The impact of individual components (e.g. ducting, bends and vent caps) on range-hood system performances was analyzed. It was found that for the flexible duct system, the ducting component has a larger influence on the total system pressure drop compared to the vent cap component. For rigid-duct range-hood systems, the impact of the vent cap component is larger than that of the rigid duct component.

Capture efficiencies based on laboratory data found in the literature are basically a function of air flow rates through the range hood for any given unit. The actual flow rates and capture efficiencies for a number of units were averaged to develop a single equation for capture efficiencies as a function of flow rate. The actual flow rate data for the actual range hood and ducting systems measured in this study were then used to find non-laboratory real-world value. The results herein found that capture efficiencies do not differ much for different duct lengths in the same configuration, with the reason being that airflow rates do not change much as the duct length changed. At the same fan speed, rigid-duct range-hood systems have higher capture efficiencies compared to flexible duct range hood systems, with capture efficiency values being 90% and 85%

respectively at high fan speeds. Of special importance, fan speeds have the largest effect on capture efficiencies with values varying from 75% to 95% for fan speeds varying from low to high.

For future range hood ducting design, it is recommended to use rigid ducts rather than flexible ducts for a better performance and a higher capture efficiency. Also, for a rigid duct ventilation system, a vent cap with smaller loss coefficients can help improve the whole system performance.

REFERENCES

Abushakra, Bass, Iain S. Walker, and Max H. Sherman. (10.3 (2004)). Compression effects on pressure loss in flexible HVAC ducts. *HVAC&R Research*, 275-289.

Abushakra, Bass, Iain S. Walker, and Max H. Sherman. (2002). *A study of pressure losses in residential air distribution systems.* Lawrence Berkeley National Laboratory (2002).

ASHRAE. (2005a). *Handbook Fundamentals.* Atlanta: American Society of Heating, Refrigerating and Air-Conditioning Engineers.

ASHRAE. (2005b). *Methods of Testing for Rating Electrically driven Unitary Air-Conditioning and Heat Pump Equipment. ANSI/ASHRAE Standard 37-2005, American Society of Heating, Refrigerating, and Air-Conditioning Engineers, Inc.*

Borson, B. (2010, March 9). *Ceiling Heights and "Scoreboard"*. Retrieved from Life of an Architect: http://www.lifeofanarchitect.com/ceiling-heights-and-scoreboard/

Burdick, A. (2011). *Advanced Strategy Guideline: Air Distribution Basics and Duct Design.* US Department of Energy, Energy Efficiency & Renewable Energy, Building Technologies Program.

Cantrill Jr, David Lee. (2013). *Static Pressure Loss in 12", 14", and 16" Non-metallic Flexible Duct. Diss.* Texas A&M University.

Delp, W. W. (2012). "Performance assessment of US residential cooking exhaust hoods.". *Environmental science & technology*, 6167-6173.

Escatel, D. S. (2011). *An Experimental Study and Analysis on Vent Cap Performance. Diss.* Texas A&M University.

HVI. (2009 , March). *HVI Publication 916, "HVI Airflow Test Procedure".* Retrieved from http://www.hvi.org/ratings/hvi916_1march2009.pdf

Klug, V. (2012). *Cooking Appliance Use in California Homes Data Collected from a Web-based Survey.*

Singer, B. C. (22.3 (2012)). Performance of installed cooking exhaust devices. *Indoor Air* , 224-234.

Uğursal, Ahmet, and C. H. Culp. (2006). Comparative Study: CFDΔ P versus MeasuredΔ P for 30% Flexible Ducts. *Proceedings of the Fifteenth Symposium on Improving Building Systems in Hot and Humid Climates.* Orlando, Florida.

Weaver, K. D. (2011). *Determining Pressure Losses For Airflow In Residential Ductwork. Diss.* Texas A&M University.

APPENDIX A

DD	cfm	Compression Ratio									
		0		4		15		30		45	
		PD	K'	PD	K'	PD	K'	PD	K'	PD	K'
6	70	0.04219	0.1488	0.10558	0.37232	0.266458	0.93967	0.47027	1.6584	0.72015	2.5396
6	80	0.0538	0.14526	0.13956	0.37682	0.352235	0.95103	0.63593	1.717	0.94564	2.5532
6	90	0.06666	0.14222	0.17852	0.38084	0.450548	0.96117	0.82988	1.7704	1.20248	2.5653
6	100	0.08076	0.13955	0.22249	0.38447	0.561531	0.97033	1.053	1.8196	1.49081	2.5761
6	110	0.09605	0.13717	0.27154	0.38778	0.685306	0.97869	1.30609	1.8652	1.81077	2.586
6	120	0.11253	0.13504	0.32569	0.39083	0.821983	0.98638	1.58993	1.9079	2.16248	2.595
6	130	0.13018	0.13311	0.385	0.39366	0.971663	0.99351	1.90519	1.948	2.54605	2.6033
6	140	0.14898	0.13134	0.4495	0.39629	1.13444	1.00016	2.25256	1.9859	2.96158	2.611
6	150	0.16891	0.12972	0.51922	0.39876	1.310402	1.00639	2.63265	2.0219	3.40916	2.6182
6	160	0.18996	0.12823	0.59419	0.40108	1.499632	1.01225	3.04606	2.0561	3.8889	2.625
6	170	0.21212	0.12683	0.67446	0.40328	1.702206	1.01779	3.49335	2.0888	4.40086	2.6314
8	140	0.03816	0.10632	0.06926	0.19298	0.190041	0.52953	0.34011	0.9477	0.6173	1.72
8	150	0.04329	0.10508	0.07978	0.19365	0.218611	0.53062	0.39205	0.9516	0.71109	1.726
8	160	0.04872	0.10394	0.09107	0.19427	0.249213	0.53165	0.44779	0.9553	0.81167	1.7316
8	170	0.05444	0.10287	0.10312	0.19486	0.28185	0.53262	0.50736	0.9588	0.91908	1.7368
8	180	0.06044	0.10188	0.11594	0.19542	0.316526	0.53354	0.57076	0.9621	1.03334	1.7418
8	190	0.06673	0.10095	0.12953	0.19595	0.353245	0.5344	0.638	0.9652	1.15446	1.7465
8	200	0.07329	0.10007	0.14389	0.19645	0.39201	0.53522	0.70911	0.9682	1.28247	1.751
8	210	0.08014	0.09924	0.15902	0.19693	0.432824	0.53601	0.78408	0.971	1.41737	1.7553
8	220	0.08726	0.09846	0.17493	0.19739	0.47569	0.53676	0.86294	0.9737	1.5592	1.7594
8	230	0.09465	0.09772	0.19162	0.19783	0.520612	0.53747	0.94569	0.9763	1.70796	1.7633
8	240	0.10232	0.09702	0.20909	0.19825	0.56759	0.53816	1.03235	0.9788	1.86367	1.767
8	250	0.11026	0.09634	0.22735	0.19866	0.61663	0.53882	1.12291	0.9812	2.02634	1.7706
8	260	0.11846	0.0957	0.24638	0.19905	0.667732	0.53945	1.2174	0.9835	2.19599	1.7741
10	200	0.02536	0.08453	0.05381	0.17937	0.096693	0.32231	0.15666	0.5222	0.25179	0.8393
10	210	0.02774	0.08388	0.05938	0.17954	0.10723	0.3242	0.17323	0.5237	0.27868	0.8426
10	220	0.03022	0.08326	0.06523	0.17971	0.118344	0.32602	0.19065	0.5252	0.307	0.8457
10	230	0.0328	0.08267	0.07136	0.17987	0.130039	0.32776	0.20893	0.5266	0.33674	0.8487
10	240	0.03547	0.0821	0.07777	0.18002	0.142317	0.32944	0.22808	0.528	0.36791	0.8516
10	250	0.03824	0.08157	0.08445	0.18017	0.155183	0.33106	0.24809	0.5292	0.40051	0.8544
10	260	0.0411	0.08106	0.09142	0.18031	0.168637	0.33262	0.26896	0.5305	0.43455	0.8571
10	270	0.04405	0.08057	0.09866	0.18045	0.182684	0.33413	0.29071	0.5317	0.47004	0.8597
10	280	0.0471	0.0801	0.10618	0.18058	0.197326	0.33559	0.31332	0.5329	0.50697	0.8622
10	290	0.05024	0.07966	0.11398	0.18071	0.212566	0.33701	0.33681	0.534	0.54536	0.8646
10	300	0.05348	0.07922	0.12206	0.18083	0.228406	0.33838	0.36117	0.5351	0.58521	0.867
10	310	0.0568	0.07881	0.13042	0.18095	0.244848	0.33971	0.38641	0.5361	0.62651	0.8693
10	320	0.06022	0.07841	0.13906	0.18106	0.261895	0.34101	0.41253	0.5371	0.66928	0.8715
10	330	0.06373	0.07803	0.14797	0.18117	0.27955	0.34227	0.43952	0.5381	0.71352	0.8736
10	340	0.06733	0.07765	0.15717	0.18128	0.297814	0.3435	0.4674	0.5391	0.75923	0.8757
10	350	0.07101	0.07729	0.16665	0.18139	0.31669	0.3447	0.49616	0.54	0.80642	0.8777
10	360	0.07479	0.07695	0.17641	0.18149	0.33618	0.34586	0.52581	0.541	0.85508	0.8797
10	370	0.07866	0.07661	0.18645	0.18159	0.356285	0.347	0.55634	0.5418	0.90523	0.8816
10	380	0.08262	0.07628	0.19677	0.18169	0.377009	0.34812	0.58776	0.5427	0.95686	0.8835
10	390	0.08666	0.07597	0.20737	0.18178	0.398352	0.3492	0.62007	0.5436	1.00998	0.8854
10	400	0.09079	0.07566	0.21825	0.18187	0.420317	0.35026	0.65326	0.5444	1.06459	0.8872

Figure 47. Data Used for Developing Pressure Drop Mathematical Model

APPENDIX B

Unit Conversion for Pressure Loss in Six Inch Circular Duct

$$\Delta P = C \cdot \frac{\rho V^2}{2}$$

$$A = 0.19635 ft^2 (\ 6"\ circular\ duct)$$

$$\rho = 0.75 \frac{lbm}{ft^3}$$

$$\frac{\Delta P}{\frac{1}{2}\rho V^2} = \frac{\Delta P}{\frac{1}{2}\left(0.075 \frac{lbm}{ft^3}\right)\left(\frac{\dot{V}}{0.19635 ft^2}\right)^2} = 1.02809 \frac{ft^7}{lbm} \frac{\Delta P}{\dot{V}^2}$$

Inserting conversion factors

$$\left(\frac{1.028 ft^7}{lbm}\right)\left(\frac{0.036 psi}{in.H_2O}\right)\left(\frac{in.H_2O}{\frac{ft^6}{min^2}}\right)\left(\frac{32.17 lbm \frac{ft}{s^2}}{1 lbf}\right)\left(\frac{144 in^2}{1 ft^2}\right)\left(\frac{3600 s^2}{1 min^2}\right) = 617234$$

where

$$1 psi = \frac{1 lbf}{(1 in)^2}$$

final version is

$$\Delta P = C \cdot \frac{\dot{V}^2}{617234}$$

Where L and D are in inch; ΔP is in $in.H_2O$; $\dot{V}$ is in cubic feet per minute

APPENDIX C

Pressure sensor calibration

The DAQ platform sent voltage signals to the computer, and the voltage signal was transferred to a pressure value by using Eq.12, where a and b are parameters to be calibrated, x is the voltage signal accepted by the computer, and y is the pressure readings reported to users. Y changed linearly with x value. The Fluke 717 1G pressure calibrator was used for pressure sensor calibration. A manometer as shown in Figure 48 was used to provide external pressure. Differential pressure transmitter can sense the pressure of air by adjusting the height of the water.

$$y = ax + b \tag{12}$$

Figure 48. Manometer Used for Reference Pressure Supply

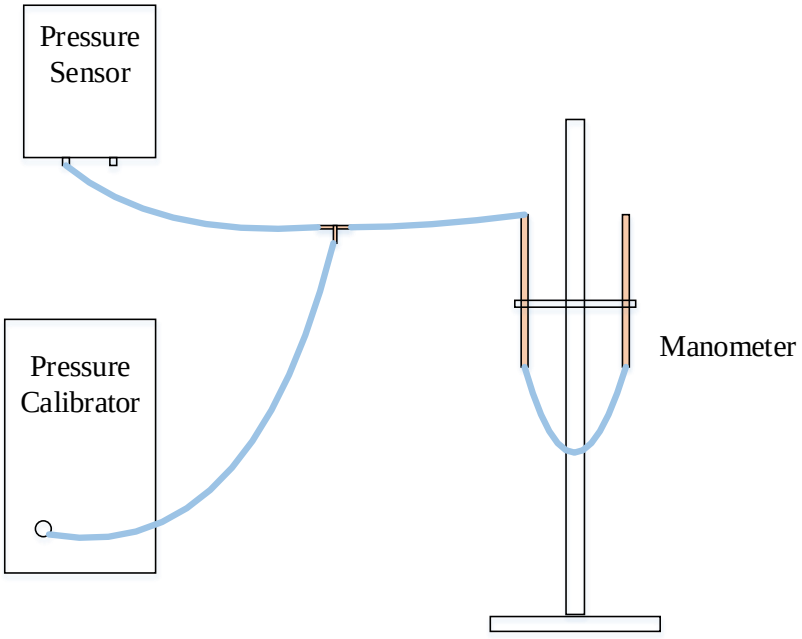

Figure 49. Tube Connection for Pressure Calibration

Figure 49 shows the tube connections for pressure calibration. The manometer was connected to the pressure calibrator (Fluke) and the pressure sensor to provide a reference pressure. Adjusting the height of the water to give a pressure supply, taking 0.5, 1, 1.5, 2, 2.5 inches of water as target static pressure, adjusting the water height, and when the readings shown on Fluke reached the target static pressure, recording the pressure value as the reference pressure, that is y value, starting the test, and the value that was measured is the voltage, namely x value. Use x and y values to generate a linear relationship between x and y by adding a trend line, and then a and b values can be decided. In this way, a pressure sensor was calibrated. It is suggested that at the beginning of everyday test, the sensors should be calibrated, and checked a couple of times during the testing period.

APPENDIX D

Figure 50. Test Setup for Case 2

APPENDIX E

Predicted and real pressure losses through the vent cap component, ducting component and the total system for all other duct lengths in Case 1 are present here.

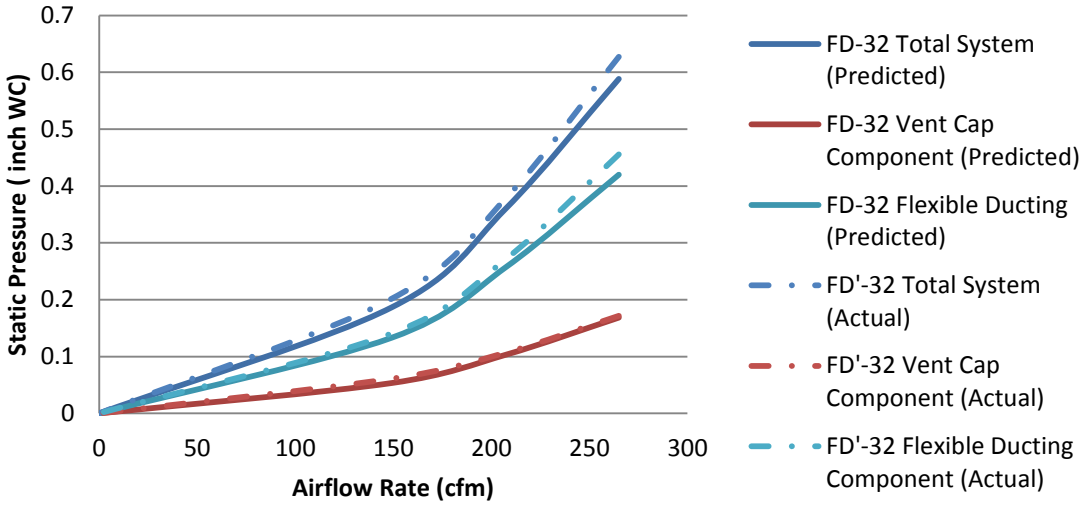

(a)

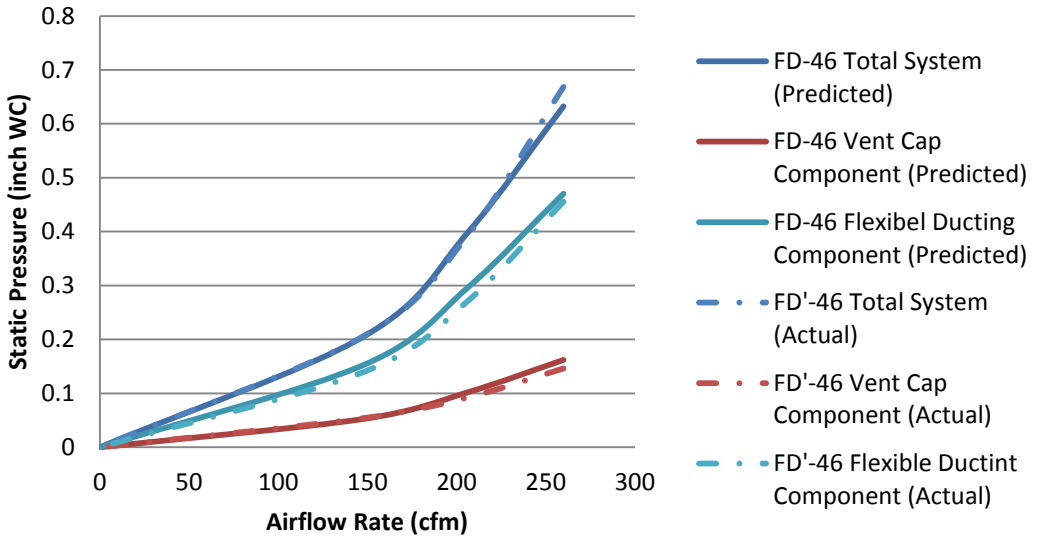

(b)

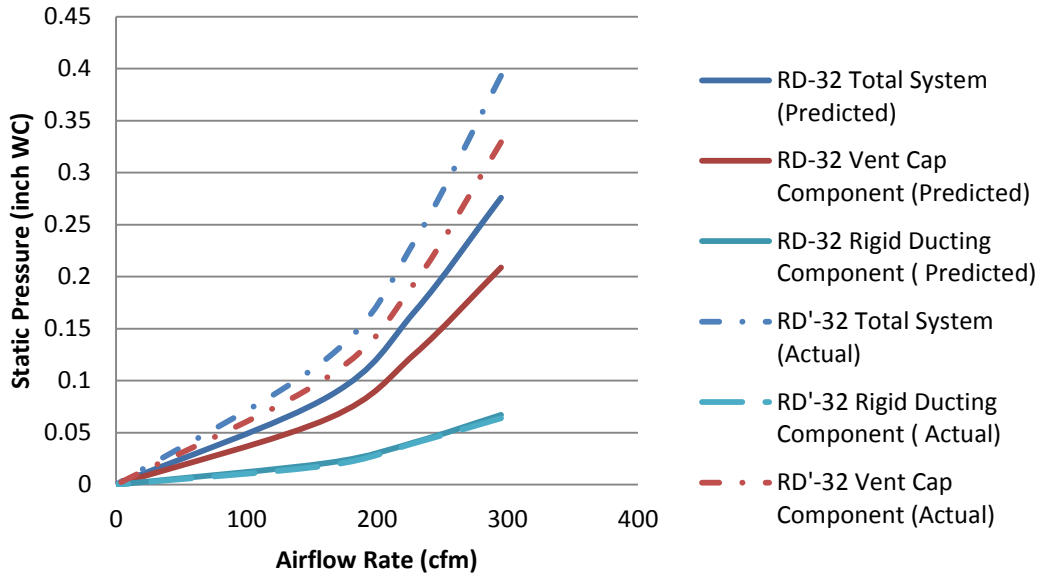
0.45
0.4
0.35
0.3
0.25
0.2
0.15
0.1
0.05
0
Static Pressure (inch WC)
0
100
200
300
400
Airflow Rate (cfm)
RD-32 Total System (Predicted)
RD-32 Vent Cap Component (Predicted)
RD-32 Rigid Ducting Component (Predicted)
RD'-32 Total System (Actual)
RD'-32 Rigid Ducting Component (Actual)
RD'-32 Vent Cap Component (Actual)

(c)

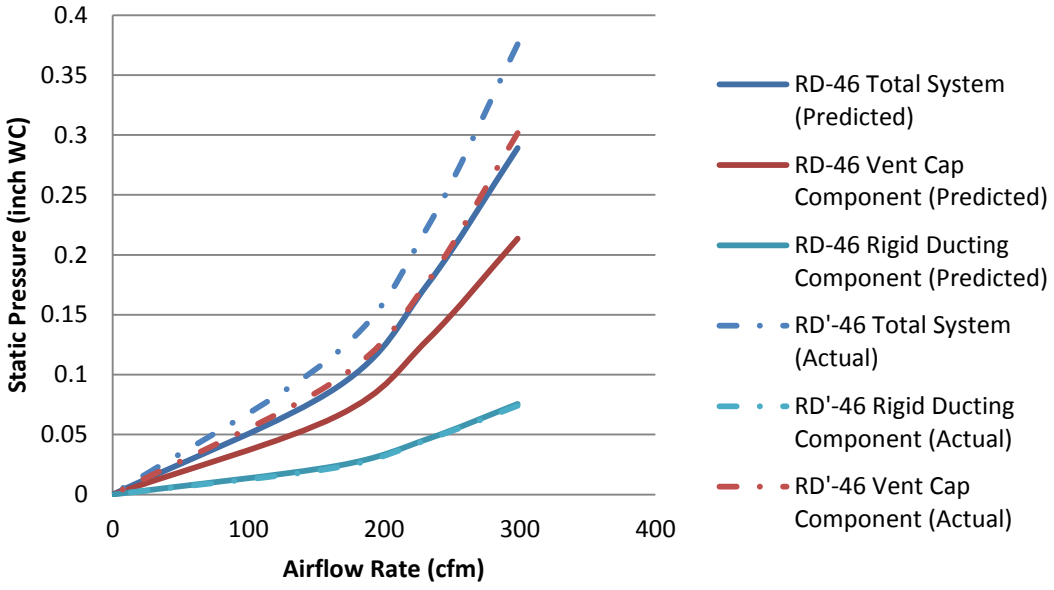
0.4
0.35
0.3
0.25
0.2
0.15
0.1
0.05
0
Static Pressure (inch WC)
0
100
200
300
400
Airflow Rate (cfm)
RD-46 Total System (Predicted)
RD-46 Vent Cap Component (Predicted)
RD-46 Rigid Ducting Component (Predicted)
RD'-46 Total System (Actual)
RD'-46 Rigid Ducting Component (Actual)
RD'-46 Vent Cap Component (Actual)

(d)

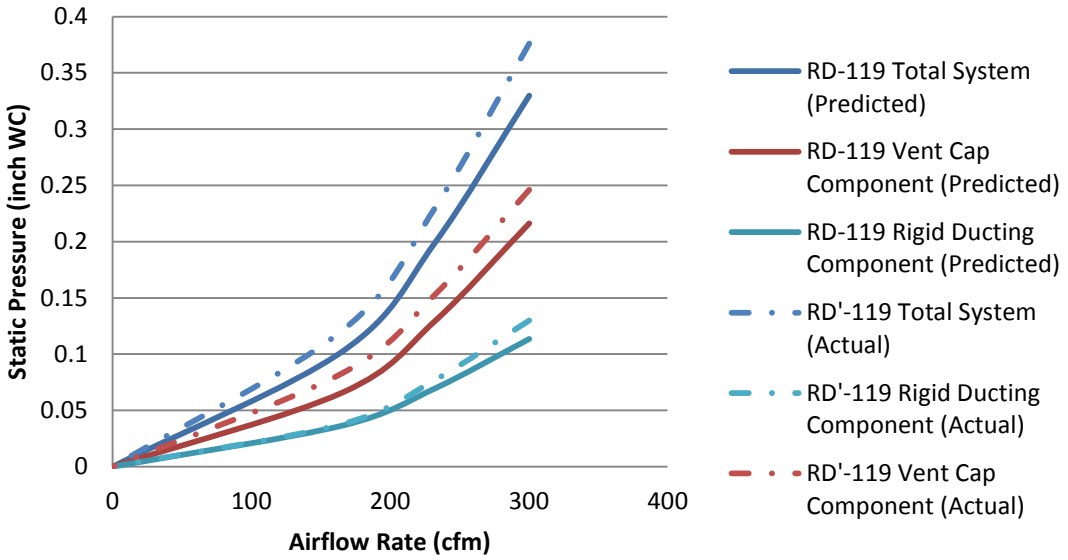

(e)

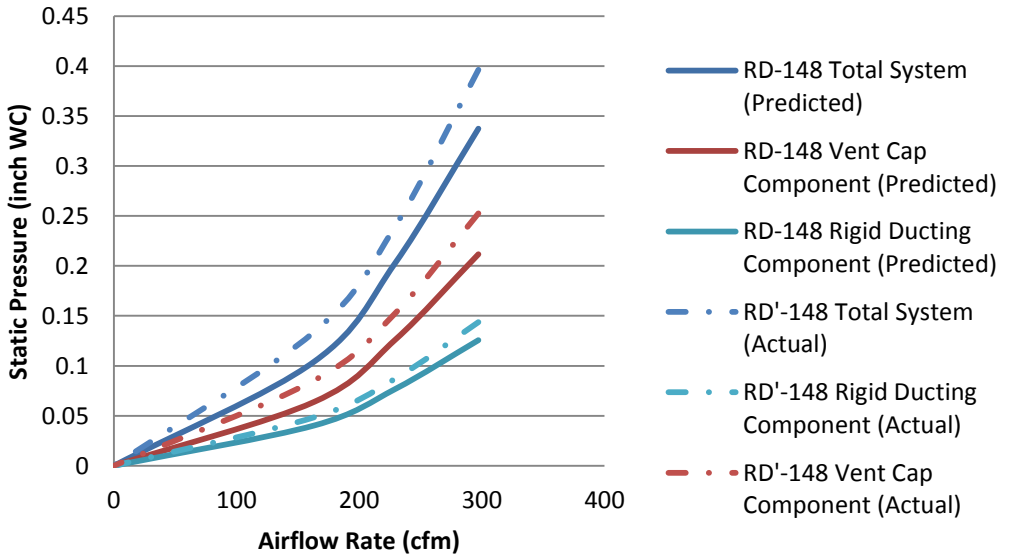

(f)

Figure 51. Actual and Predicted Pressure Loss for Components, and Total System for Case 1, (a) 32" Flex Duct; (b) 46" Flex Duct; (c) 32" Rigid Duct, (d) 46" Rigid Duct, (e) 119" Rigid Duct, (f) 148" Rigid Duct